Environmental Chemistry Letters
https://doi.org/10.1007/s10311-024-01732-4

REVIEW ARTICLE

Carbon–neutral hydrogen production by catalytic methane decomposition: a review

Dwi Hantoko[1,2] · Wasim Ullah Khan[1,2] · Ahmed I. Osman[3] · Mahmoud Nasr[4] · Ahmed K. Rashwan[5] · Yahya Gambo[1] · Ahmed Al Shoaibi[6] · Srinivasakannan Chandrasekar[6] · Mohammad M. Hossain[1,2]

Received: 22 February 2024 / Accepted: 3 March 2024

Abstract

The global hydrogen demand is projected to increase from 70 million tons in 2019 to more than 200 million tons in 2030. Methane decomposition is a promising reaction for H_2 production, coupled with the synthesis of valuable carbon nanomaterials applicable in fuel cell technology, transportation fuels, and chemical synthesis. Here, we review catalytic methane decomposition, with focus on catalyst development, deactivation, reactivation, regeneration, and on economics. Catalysts include mono-, bi-, and trimetallic compounds and carbon-based compounds. Catalyst deactivation is induced by coke deposition. Despite remarkable strides in research, industrialization remains at an early stage.

Keywords Hydrogen production · Methane decomposition · Metal-based catalyst · Deactivation · Carbon nanomaterials · Economic evaluation

Introduction

Fulfilling the world's energy needs currently relies heavily on the consumption of fossil fuels, presenting two critical challenges: the depletion of these finite resources and the escalating emission of greenhouse gases (Sánchez-Bastardo et al. 2021; Osman et al. 2023a). While renewable energy sources offer a sustainable alternative, their widespread implementation is hindered by technological complexities, high operational costs, and concerns regarding long-term feedstock supply chain sustainability (Sgouridis et al. 2019; Li et al. 2020). To address these challenges and minimize emissions, the focus must shift to optimizing existing technologies that efficiently utilize fuel and reduce emissions (Osman et al. 2023b).

Hydrogen emerges as a promising energy carrier, being lightweight, abundant, and environmentally friendly, offering a sustainable alternative that reduces greenhouse gas emissions (Mason 2007; Lepage et al. 2021). Although hydrogen is extensively used in industry for ammonia synthesis and oil refining, its future applications in transportation, power generation, and construction present a growing demand for pure hydrogen. However, the clean image of hydrogen is somewhat tarnished by the greenhouse gas emissions associated with its production (IRENA 2019; Osman et al. 2022; Nikolaidis and Poullikkas 2017). Despite the decreasing cost of power production from renewable sources, the financial challenges involved mean that natural gas-based hydrogen manufacturing technologies will likely persist to meet the surging hydrogen demand (Osman et al. 2023c).

✉ Ahmed I. Osman
aosmanahmed01@qub.ac.uk

✉ Mohammad M. Hossain
mhossain@kfupm.edu.sa

1 Interdisciplinary Research Center for Refining and Advanced Chemicals, King Fahd University of Petroleum and Minerals, 31261 Dhahran, Saudi Arabia

2 Department of Chemical Engineering, King Fahd University of Petroleum and Minerals, 31261 Dhahran, Saudi Arabia

3 School of Chemistry and Chemical Engineering, Queen's University Belfast, David Keir Building, Stranmillis Road, Belfast BT9 5AG, Northern Ireland, UK

4 Nanocomposite Catalysts Lab., Chemistry Department, Faculty of Science at Qena, South Valley University, Qena 83523, Egypt

5 Department of Food and Dairy Sciences, Faculty of Agriculture, South Valley University, Qena 83523, Egypt

6 Department of Chemical Engineering, Khalifa University of Science and Technology, Abu Dhabi, United Arab Emirates

Published online: 20 April 2024

Various methods contribute to hydrogen production, such as steam/dry reforming of methane (Franchi et al. 2020; Aramouni et al. 2018), water splitting (Voitic and Hacker 2016), catalytic methane decomposition (Alves et al. 2021), partial oxidation of methane or oil (Arku et al. 2018), and coal/biomass gasification (Alptekin and Celiktas 2022). Water splitting and biomass gasification processes will not become competitive until governments impose carbon fees, and research is expanded to increase economic viability (Nikolaidis and Poullikkas 2017; Deka et al. 2022). Among these methods, catalytic methane decomposition emerges as an environmentally benign method, producing pure hydrogen without carbon dioxide emissions and valuable carbon material. Though mildly endothermic, it demands lower total energy compared to other methods, thereby reducing operational costs. However, catalyst deactivation due to carbon deposition and metal sintering remains a bottleneck issue.

The novelty of this review is to offer a comprehensive exploration of catalytic methane decomposition catalyst development, delving into catalytic reaction mechanisms and materials. While reactor design is integral to this technology, its discussion is omitted, focusing instead on the current development of catalytic methane decomposition catalysts, investigating deactivation behaviors, regeneration systems, economic potential, and providing insights into challenges and future developments. All sections of this review paper are illustrated in Fig. 1.

Hydrogen production processes

Steam reforming of methane (SRM), dry reforming of methane (DRM), and partial oxidation of methane (POM) are recent thermochemical techniques for producing hydrogen from methane, the main component of natural gas. While steam reforming constitutes the major global industrial process, accounting for approximately 95% of total global hydrogen production (Ighalo and Amama 2024), dry reforming of methane presents a promising solution by converting both methane and carbon dioxide into valuable hydrogen-rich syngas. However, the current catalyst systems for dry reforming of methane involve expensive noble metals such as platinum, ruthenium, and rhodium (Al-Fatesh et al. 2025). Partial oxidation of methane has been a subject of research for over half a century, but it has not found widespread applications in gas-to-liquid processes. Recently, the partial oxidation of methane has gained significance in petroleum and allied chemical industries for hydrogen gas production. This process converts methane into syngas (hydrogen + carbon monoxide), leading to the production of crucial chemical products (Kumar et al. 2009).

Autothermal reforming, a hybrid process combining partial oxidation with conventional steam reforming, presents an innovative approach to hydrogen production. By eliminating the need for an external heat source, this method offers the potential to enhance the thermal conversion efficiency of hydrogen production while simultaneously reducing operational costs (Carapellucci and Giordano 2020). On the other hand, catalytic methane decomposition has emerged as a promising technology for environmentally friendly hydrogen production. This reaction exclusively yields hydrogen in the gas-phase and solid-phase carbon, simplifying the process by eliminating the need for product separation and mitigating carbon dioxide emissions. Furthermore, catalytic methane decomposition is characterized by its moderate endothermic nature, resulting in lower total energy and heat demands compared to traditional steam reforming and dry reforming methods. This reduction in energy requirements is crucial for lowering operating temperatures and equipment costs (Zhang et al. 2017). A summary of the key hydrogen-generating processes from methane is provided in Table 1.

Despite high efficiency and low cost, they produce significant COx emissions and require more energy. The high cost of equipment and the purification of hydrogen limit its industrial applicability. Additionally, fuel reforming involves carbon monoxide removal through water gas shift reaction and selective oxidation, causing large amounts of carbon monoxide in post-reaction mixtures even after purification. As a result, catalytic methane decomposition developed attention as a unique technology for environmentally benign hydrogen generation. This technology is still in the development stage and requires further attention.

Catalytic methane decomposition

Because of the strong C–H bond (440 kJ/mol) and greater molecular structural symmetry, the thermal decomposition of methane takes place at higher temperatures (greater than 1300 °C) without the presence of a catalyst (Mitoura dos Santos Junior et al. 2022). The presence of a suitable catalyst is believed to reduce the activation energy and decrease the reaction time at lower temperatures (450–750 °C) (Ashik et al. 2015). Many researchers have explored the proper catalyst for catalytic methane decomposition reaction at different ranges of operating conditions, yet the pathway to make the industrially competitive catalytic methane decomposition still needs to be developed. Various catalysts, including metals and carbon-based catalyst and their modification, were applied to enhance the methane conversion, selectivity, hydrogen yield, and to increase the catalytic stability. Transition metals such as noble and non-noble metals are well known to be the most active site for catalyst. The detailed catalytic performance along with reaction conditions of some of the mono- and bi-metallic catalysts for catalytic methane decomposition process is summarized in Table 2.

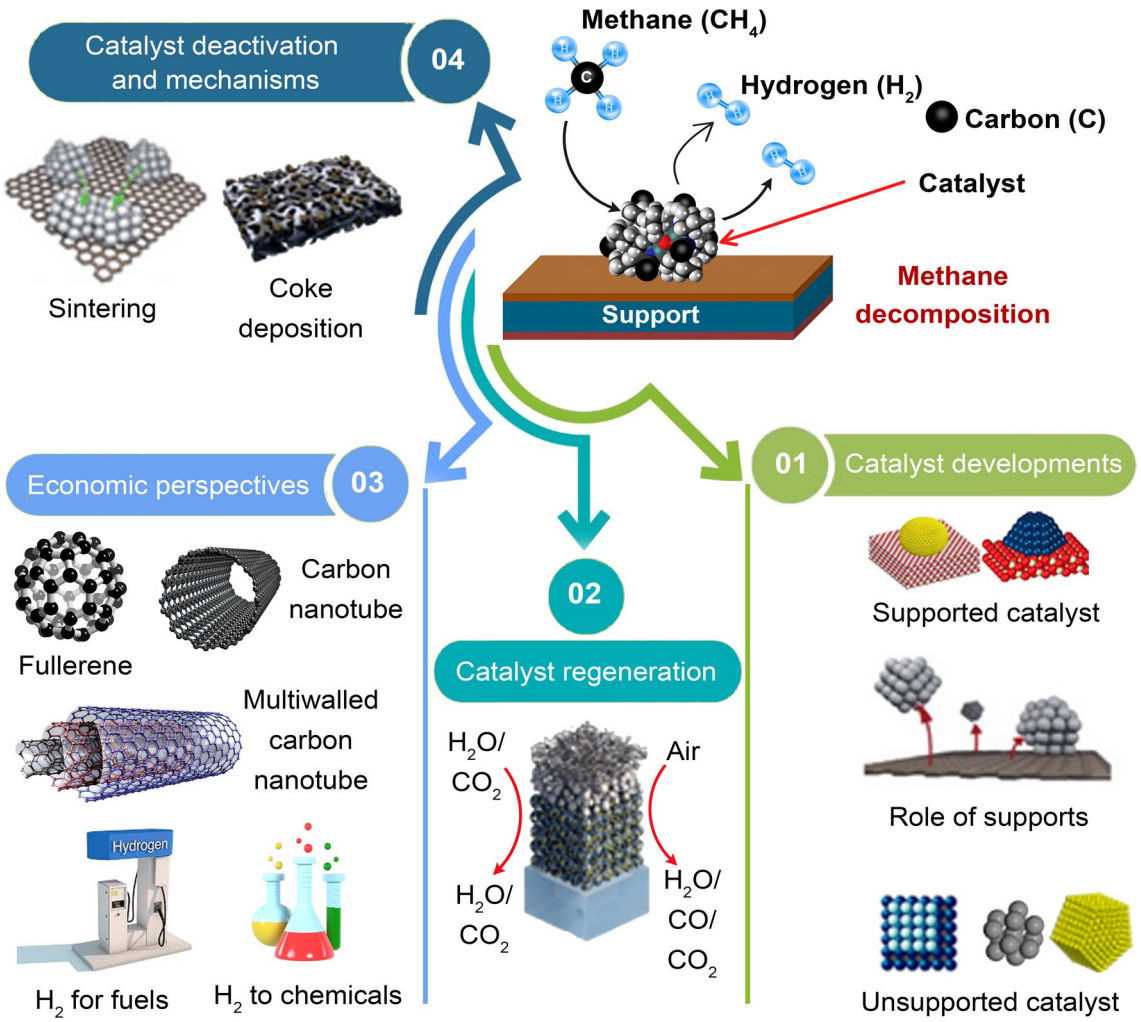

Fig. 1 Content of this review on catalytic methane decomposition. This figure provides a concise summary of the key aspects covered in the review paper on catalytic methane decomposition. The figure highlights various important topics related to catalytic methane decomposition, including catalyst development, deactivation behaviors, regeneration techniques, economic considerations, and future developments. The central theme of the figure revolves around the catalytic process of methane decomposition and its significance in the context of carbon capture and storage (CCS). The figure emphasizes the role of catalysts in facilitating the decomposition of methane into valuable products, such as hydrogen and carbon nanomaterials, while also addressing the challenges associated with catalyst deactivation. Furthermore, the figure sheds light on the strategies and techniques employed for catalyst regeneration, which are crucial for maintaining catalyst activity and prolonging its lifespan. It also touches upon the economic aspects of methane decomposition, highlighting its potential as a sustainable and cost-effective process for energy production

Catalyst development

Metal-based catalysts

Monometallic catalysts

Nickel-based metal is widely used in catalytic processes involving methane steam reforming and dry methane reforming. Monometallic, bimetallic, and part of mixed nickel metallic were widely used for methane decomposition processes (Hasnan et al. 2020; Ping et al. 2016; Pudukudy et al. 2017; Shen and Lua 2015). The unsupported nickel oxide (NiO) prepared by the facile method showed highly active and relatively stable for 360 min for methane decomposition reaction. The maximum hydrogen yield of 66% was observed, and bulk metal encapsulated carbon nano chunks were deposited on the surface of the nickel oxide catalyst (Pudukudy et al. 2016). The magnetic property of a non-supported catalyst facilitates easier regeneration and separation of the catalyst (Fan et al. 2021). Ni/Al_2O_3 was successfully synthesized using the modified sol–gel method, and promising results were obtained.

The catalyst showed a high methane conversion of 78.8% achieved after five cycles and created base growth carbon

Table 1 Comparison between existing and potential hydrogen production methods reveal the dominance of natural gas or methane-based reforming, a well-established technology widely employed at an industrial scale

Process	Reaction	Operating conditions	Typical catalysts	Energy efficiency	Existing plant	Highlights
Dry reforming	$CH_4 + CO_2$? $2CO + 2H_2$?$H°$ = + 247 kJ/mol	Greater than 600 °C	Ni-based	Not available	Linde pilot reformer is located in Pullach, Germany	The feed comprises two major greenhouse gases. Catalysts used must be capable of activating the C–H bond in methane and the C–O bond in carbon dioxide. A significant challenge lies in catalyst deactivation due to the blockage of active sites by carbon. Promising alternatives to alleviate this problem include modulation of support acid–base properties, optimization of the size and dispersion of the active phase, and the development of core–shell catalysts. Additionally, the reaction $CO_2 + H_2$? $H_2O + CO$ may reduce the hydrogen generated in the process
Steam reforming	$CH_4 + H_2O$? $CO + 3H_2$?$H°$ = + 206 kJ/mol	Greater than 700 °C	Ni-based	83%	(1) Topsoe package hydrogen plants at Air Liquide, Belgium; plants in the USA (2) Air Liquide steam methane reformer, Chempark Dormagen site, Germany	Higher hydrogen concentration due to an additional hydrogen production achieved through reverse water gas shift reaction (RWGS) ($CO + H_2O$? $CO_2 + H_2$?$H°$ = - 41 kJ/mol). Its catalysts are prone to deactivation due to carbon formation or the presence of sulfur impurities in feed or sintering of active phase at elevated temperature. It has the highest carbon dioxide emission per kg of hydrogen produced

Table 1 (continued)

Process	Reaction	Operating conditions	Typical catalysts	Energy efficiency	Existing plant	Highlights
Partial oxidation	$CH_4 + 0.5O_2$? $CO + 2H_2$?$H°$ = - 36 kJ/mol	Less than or equal to 600 °C	Not available	70–80%	Pearl GTL, Ad-Da?irah, Qatar	It can be driven thermally or catalytically at lower temperatures. Co-feeding carbon dioxide reduces the H_2/CO ratio. It is robust to sulfur impurities in the feed. However, soot formation, the potential for hotspot formation, and the high cost of pure oxygen are some of its challenges
Autothermal reforming	Partial oxidation of methane, steam reforming of methane, and the enthalpy of the reaction depend on the feed composition	Greater than 2500 °C $H_2O/C = 0.5–3.5$, $O_2/C = 0.4–0.6$	Ni-based ($Ni/MgAl_2O_4$) Noble metal-based (Ru, Pt, and Rh)	71–74%	OLTIN YO'L GTL, Shurtan Gas and chemical complex, Karshi, Uzbekistan	Integrates steam reforming with partial oxidation, and its main obstacle lies in the development of a robust reactor configuration coupled with catalyst design for minimal transport limitation. It offers ease of heat energy integration and presetting H_2/C in the product via modulation of the feed composition
Thermal decomposition	CH_4 + energy ? $C_{(s)} + 2H_{2(g)}$?$H°$ = + 74 kJ/mol	Greater than 1000 °C	Not involving catalyst	Not available	(1) Monolith demonstration plant, California (2) Monolith commercial plant in Nebraska, USA	Various alternative heating sources, such as plasma, microwave, and dielectric barrier discharge, could be utilized. Innovative reactor designs remain the focus in the development of the process. Its current commercial drive is mainly due to carbon black production. However, its bottlenecks include low-energy efficiency and difficulty in narrow carbon specifications

Table 1 (continued)

Process	Reaction	Operating conditions	Typical catalysts	Energy efficiency	Existing plant	Highlights
Catalytic decomposition	$CH_{4(g)}$? $C_{(s)} + 2H_{2(g)}$ $?H^{\circ} = +74$ kJ/mol	Less than 1000 °C	Ni-, Pt-, Fe-, Co-, Pd-, Cu-based and carbonaceous catalysts	Not available	Research level	Deactivation due to coke deposition is the main problem of metal-based catalysts. Carbonaceous catalysts are generated during the reaction, and the process appears auto-catalyzed and more economical. Nonetheless, changes in the microstructure of the carbon cause a significant decline in initial activity

Ongoing attention is directed toward refining catalysts and optimizing operational parameters to enhance the efficiency of methane-based reforming processes. Environmental imperatives, particularly concerning global warming, are fueling the exploration of cleaner hydrogen production technologies as alternatives to conventional methane reforming. The quest for sustainable solutions underscores the urgency of research and development efforts aimed at advancing cleaner and more environmentally friendly methods of hydrogen production. The details for the reactions were obtained from Aramouni et al. (2018) and Pham Minh et al. (2021). Energy value of the hydrogen produced/energy input for the production. The values are derived from McHugh et al. (2005)

nanotubes (Gao et al. 2019b). Bayat et al. (2015) discussed the development and characterization of Ni-based catalysts supported on mesoporous nanocrystalline gamma alumina (?-Al_2O_3) for methane thermocatalytic decomposition to produce CO*x*-free hydrogen and carbon nanofibers. The catalysts were prepared with different nickel loadings, and their activity and stability were investigated. The results showed that the catalysts with different nickel contents exhibited a mesoporous structure with a high surface area. Increasing the nickel content led to a decrease in pore volume and an increase in crystallite size. The catalytic performance of the prepared catalysts was influenced by both the nickel content and the operating temperature. The initial conversion of catalysts increased with an increase in reaction temperature but significantly decreased the catalyst lifetime. Scanning electron microscopy analysis of the spent catalysts revealed the formation of intertwined carbon filaments, with higher reaction temperatures leading to smaller nanofiber diameters and increased formation of encapsulating carbon. The activity of the Ni-based catalysts was found to be higher compared to other metals such as cobalt and iron group metals. Nickel exhibited sufficient activity for methane thermocatalytic decomposition, and its catalytic activity was higher than that of cobalt and iron. The mechanism of methane decomposition and carbon fiber growth involved the detachment of the catalyst particle from the support, forming a filament with the catalyst particle on the filament's tip. In another study conducted by Karaismailoglu et al. (2019), yttria (Y_2O_3)-supported nickel exhibited stable activity at higher temperatures due to the enhanced surface area.

In this study, the catalysts were prepared using the sol–gel citrate method and characterized using various techniques. Activity tests were conducted in a tubular reactor, and the results were compared to non-catalytic reactions. The findings reveal that the presence of the catalyst significantly influenced methane conversion. Without a catalyst, methane decomposition did not occur until a temperature of 880 °C was reached. However, with the introduction of the catalyst, methane conversion of 14% was achieved at 500 °C. As the reaction temperature increased, coke formation also increased. Catalysts with lower nickel content exhibited reduced carbon formation. Notably, a catalyst with yttria support demonstrated stable activity at higher temperatures. The authors highlight that the enhanced surface area of the yttria-supported nickel catalyst contributed to its stable activity. They suggest that doping nickel-based catalysts with yttria can improve their activity and stability in catalytic methane decomposition. This research provides valuable insights into the potential of catalytic methane decomposition as a green process for hydrogen production, with the yttria-supported nickel catalyst showing promise for stable activity at higher temperatures.

Table 2 Catalytic activity of various metal-based catalysts at different reaction conditions during catalytic methane decomposition

Catalyst	Synthesis strategy	Temperature (°C)	Reaction time (h)	Hydrogen yield (%)	Methane conversion (%)	Carbon type	Highlight on the catalytic methane decomposition performance	References
NiO	Facile precipitation	800	360	66	Not available	Irregular shape carbon chunks	Unsupported nickel oxide exhibited loose aggregation and was very active and stable for the process	Pudukudy et al. (2016)
Fe_2O_3	Facile precipitation	800	260	52	Not available	Graphene sheets	The well-packed particle arrangement was found on the unsupported iron oxide catalyst. Fe-based catalyst gave high catalytic stability owing to its high carbon diffusion	Pudukudy et al. (2016)
Fe/Al_2O_3	Incipient wet impregnation	800	180	Not available	85	Carbon nanofibers	The reduction of iron oxide precursors significantly impacts catalyst stability and hydrogen yield. Impregnation-produced larger iron particles maintain stable activity outside carbon fibers, enhancing catalyst stability	Fakeeha et al. (2018a)
$Ni/CeO_2–Al_2O_3$	Co-precipitation	700	400	53	Not available	Carbon nanofibers and carbon nanotubes	Ceria content has a considerable impact on catalytic activity. Over the $Ni/Ce_{25}–Al_{75}$, the maximum methane conversion was obtained. The development of a Ni–O–Ce solid solution aids in the dispersion of relatively small Ni-particles, which contributes to the production of filamentous carbon	Ahmed et al. (2016)

Table 2 (continued)

Catalyst	Synthesis strategy	Temperature (°C)	Reaction time (h)	Hydrogen yield (%)	Methane conversion (%)	Carbon type	Highlight on the catalytic methane decomposition performance	References
Ni–Pd/Al_2O_3	Sol–gel	700	600	Not available	95	Carbon nanofibers	Ni–Pd alloy increased catalytic activity and facilitated carbon diffusion in Ni–Pd. Ni–Pd catalyst has a faster carbon diffusion rate, preventing encapsulating carbon development and prolonging catalyst life	Bayat et al. (2016a)
Ni–Fe/Al_2O_3	Sol–gel	700	600	Not available	70	Carbon nanofibers and carbon nanotubes	The iron addition enhanced the catalyst stability by improving the carbon diffusion rate and inhibiting encapsulating carbon formation	Bayat et al. (2016b)
Ni–Co/Al_2O_3	Sol–gel	650	80	Not available	69.3	Carbon nanotubes	A less significant sintering phenomenon was also found in bimetallic catalysts	Gao et al. (2019a)
Ni–Mn–Ru/Al_2O_3	Impregnation	750	240	Not available	93.76	Carbon nanofibers	Ruthenium content affects catalyst activity through texture changes, leading to rapid deactivation due to a higher carbon deposition rate on catalyst surfaces compared to reaction carbon diffusion	Wang et al. (2020)
Ni–Co/Al_2O_3·TiO_2	Sol–gel	650	80	Not available	72.5	Carbon nanotubes	The bimetallic catalyst exhibits higher methane conversion compared to monocatalyst due to its resistance to sintering	Gao et al. (2019a)

Table 2 (continued)

Catalyst	Synthesis strategy	Temperature (°C)	Reaction time (h)	Hydrogen yield (%)	Methane conversion (%)	Carbon type	Highlight on the catalytic methane decomposition performance	References
Ni–Cu/Al Molten salt	Fusion	650	120	Not available	Not available	Carbon nanofibers	Lattice constant and particle size distribution depend on copper loading; $Ni_{(x)}Cu_{(x-1)}$ solid solution formation forms fishbone carbon nanofibers with diverse morphological properties	Torres et al. (2018a)
Ni-Pd/SBA-15	Hydrothermal and impregnation	700	420	59	Not available	Multi-walled carbon nanotubes	Palladium addition on Ni-SBA-15 enhances nickel oxide crystallinity, fine dispersion, and surface area, resulting in excellent catalytic activity of Pd-based catalyst with Ni–Pd bimetallic species	Pudukudy et al. (2015)
Co–Fe/Al_2O_3	Incipient wet impregnation	700	180	72	73	Carbon nanofibers	The catalyst demonstrated excellent catalytic activity due to its suitable combination of metal dispersion, support interaction, and reducible species	Al-Fatesh et al. (2016)
Fe/$CeZrO_2$	Wetness impregnation	700	125	83	85	Carbon nanotubes	The unpromoted iron catalyst showed high initial activity but decreased over time due to lower surface area and coke-like carbon formation, causing rapid deactivation	Ramasubramanian et al. (2020)

Table 2 (continued)

Catalyst	Synthesis strategy	Temperature (°C)	Reaction time (h)	Hydrogen yield (%)	Methane conversion (%)	Carbon type	Highlight on the catalytic methane decomposition performance	References
Fe–Mo/$CeZrO_2$	Wetness impregnation	700	125	90	90	Carbon nanotubes	The addition of molybdenum increased the Fe-based catalyst surface area, ensuring stability after two regeneration cycles in Fe–Mo/$CeZrO_2$	Ramasubramanian et al. (2020)
Fe–Co/$CeZrO_2$	Wetness impregnation	700	125	90	90	Bamboo-shaped nanostructures and chain-like nanocarbons	Co-promoter addition on Fe-based catalysts improved catalytic activity, producing higher carbon content than unpromoted Fe/$CeZrO_2$ catalysts	Ramasubramanian et al. (2020)
Fe–Ni/$La_2O_3{\cdot}ZrO_2$	Wetness impregnation	800	240	84	92	Amorphous and filamentous graphitic carbon	Nickel addition increased catalyst surface area, improved metal particle dispersion, enhanced methane conversion, and improved catalyst stability	Fakeeha et al. (2020)
Fe–Co/MgO	Co-impregnation	700	570	90	Not available	Multi-walled carbon nanotubes	Iron and cobalt particles could block magnesium oxide pores, forming a nonporous structure, resulting in effective and stable hydrogen production through Fe–Co/MgO	Awadallah et al. (2014a)

Table 2 (continued)

Catalyst	Synthesis strategy	Temperature (°C)	Reaction time (h)	Hydrogen yield (%)	Methane conversion (%)	Carbon type	Highlight on the catalytic methane decomposition performance	References
Ni–Cu–Zn/MCM-22	Wetness impregnation	750	50	Not available	87	Carbon nanotubes	The metal combination (Ni–Cu–Zn) showed higher catalytic activity for the decomposition reaction and produced a high yield of carbon nanotubes Copper and zinc prevented agglomeration and increased nickel nanoparticle dispersion, promoting carbon nanotube formation	Saraswat and Pant (2013a)
Fe–Ni–Co/Al_2O_3	Incipient wet impregnation	700	180	Not available	70	Carbon nanofibers	The surface area and pore diameter reduced after nickel, cobalt, and iron impregnation, which was attributed to the partial blocking of the pore by the metal particles	Al-Fatesh et al. (2016)
Fe–Ni–Cu/Al_2O_3	Sol–gel	750	600	Not available	82	Carbon nanofibers	Copper enhanced catalytic performance at higher temperatures by promoting methane adsorption and carbon migration, but initial methane conversion decreased with increased copper content	Bayat et al. (2016c)

Table 2 (continued)

Catalyst	Synthesis strategy	Temperature (°C)	Reaction time (h)	Hydrogen yield (%)	Methane conversion (%)	Carbon type	Highlight on the catalytic methane decomposition performance	References
Fe–Mo–Cu/MgO	Impregnation	900	30	Not available	Not available	Single-walled carbon nanotubes	Fe–Mo or Fe–Mo–Cu/MgO catalysts yielded higher yields and quality single-walled carbon nanotubes than monometallic Fe/MgO catalysts. Molybdenum prevented surface aggregation, enhancing catalytic growth activity by reducing metal particle size distribution	Awadallah et al. (2017a)

Each entry includes details such as the synthesis method, reaction temperature, reaction time, hydrogen yield percentage, methane conversion percentage, type of carbon produced, and notable findings from the catalyst's performance. The synthesis strategies range from facile precipitation to sol–gel methods, and the catalysts include metal oxides and bimetallic compositions supported on different substrates. The catalytic performance is assessed based on factors such as activity, stability, and carbon diffusion rate, with insights provided into the catalyst's effectiveness in hydrogen production and carbon nanomaterial formation

Similarly, the catalytic activity of Ni-based catalysts was also affected by the particle size of nickel metal (Liang et al. 2020). The larger particles of nickel could maintain the catalytic activity, while smaller particles of nickel caused rapid deactivation of the catalyst. Moreover, larger nickel particles promoted the formation of carbon nanotubes, while smaller nickel particles led to the formation of encapsulated carbon, as shown in Fig. 2. However, Ni-based catalyst suffers sintering and particle agglomeration at high temperatures above 650 °C, resulting in fast deactivation. Coke deposition is another issue in the utilization of nickel-based catalysts. Therefore, significant efforts are needed to modify the surface of a nickel catalyst to have better performance and be more stable for harsh operating conditions.

Fe-based catalysts have become the second alternative for catalytic methane decomposition and have gained great attention recently due to their catalytic activity and better stability at higher operating conditions (Fakeeha et al. 2018a; Karaismailoglu et al. 2020; Tezel et al. 2019; Torres et al. 2012). Alumina-supported iron catalyst has been synthesized and reported to have good catalytic activity, and the support materials could enhance the performance. Fakeeha et al. (2018a) synthesized the Fe/Al_2O_3 catalyst and observed that the iron catalyst gave good catalyst activity. In this study, the catalysts were prepared using different methods, including impregnation and co-precipitation, and calcined at various temperatures ranging from 300 to 800 °C. The performance of the catalysts was evaluated through various characterization techniques. The results indicate that the optimal calcination temperature for both impregnated and co-precipitated catalysts is 500 °C. The type of iron oxide precursor on the alumina support significantly influences the catalyst's performance for methane decomposition. The study highlights that Fe-based catalysts show promise for catalytic methane decomposition. The formation of various iron oxides, such as magnetite, maghemite, wustite, hematite, and spinel structures, during the calcination process plays a crucial role in the catalyst's activity. The reduction of iron oxides by hydrogen during pre-reduction treatments and high-temperature methane pyrolysis leads to the formation of partially reduced iron oxide or iron metal, which acts as the active catalytic species. Overall, the research provides valuable insights into the preparation and performance of Fe-based catalysts for hydrogen production via methane decomposition. The findings contribute to the development of efficient and environmentally friendly energy production processes. Furthermore, the activity of the iron catalyst over different supports has been tested for the catalytic methane decomposition process (Al_2O_3, SiO_2, and $MgSiO_3$) (Zhou et al. 2017). The result showed that Fe/Al_2O_3 exhibited the highest methane conversion. The Al_2O_3 support played a role in the iron crystallization to expose more Fe^0 out of the

surface area for the formation of carbon nanotubes, which was important for the catalyst activity.

Pudukudy et al. (2019) compared the catalytic performance of Fe/CeO_2 and Fe/La_2O_3 for methane decomposition reaction. In this study, the catalysts were prepared using a co-precipitation method and characterized using various analytical techniques. The results showed that both catalysts exhibited high catalytic activity and stability for methane decomposition. The Fe/CeO_2 catalyst demonstrated superior catalytic stability, with the highest initial and final hydrogen yield remaining nearly constant throughout the reaction. The catalyst yielded a maximum hydrogen yield of 66 ± 1% at 800 °C. On the other hand, the Fe/La_2O_3 catalyst experienced a substantial drop in the hydrogen yield over the

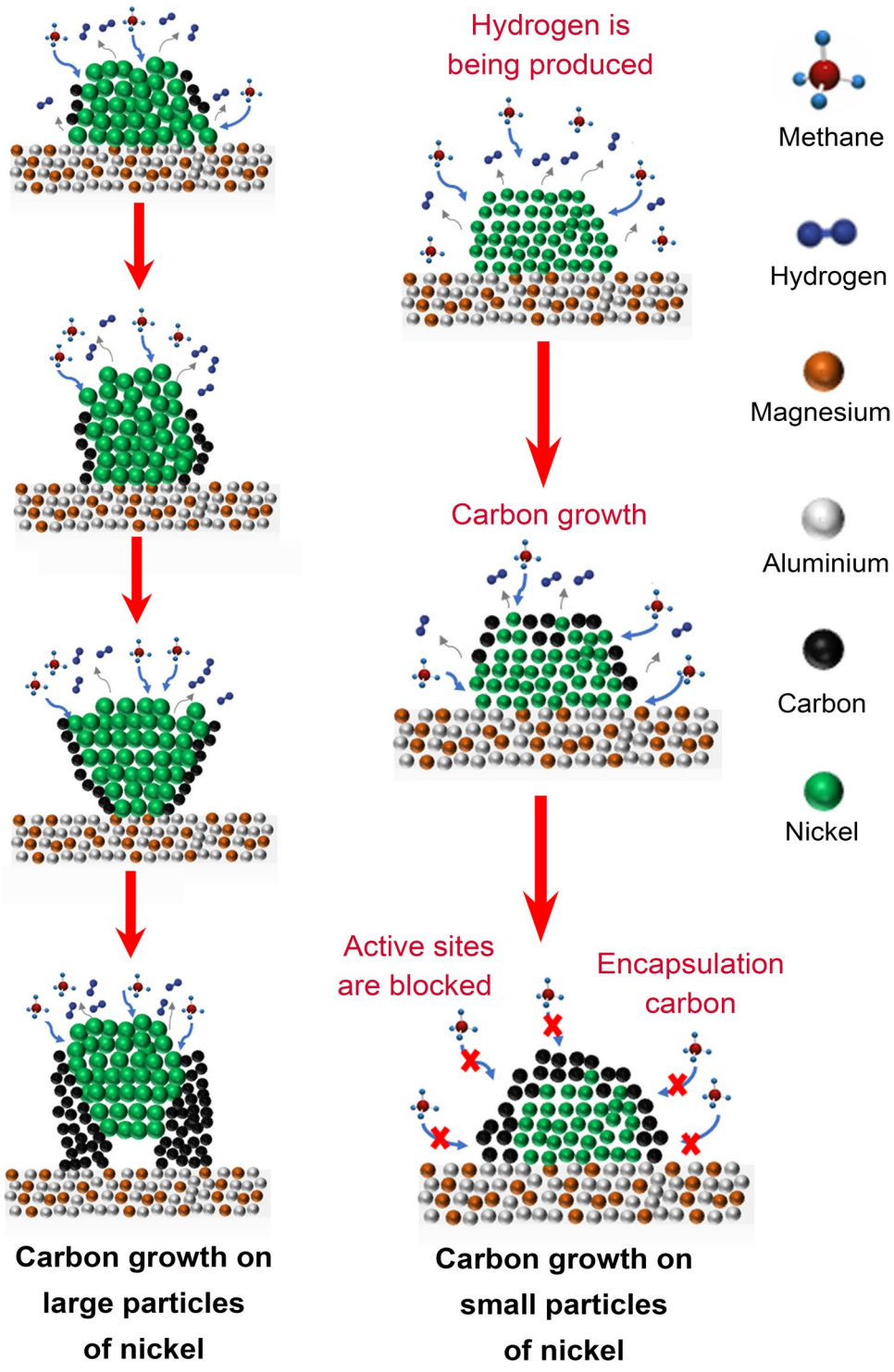

Fig. 2 Possible mechanism for the growth of carbon nanotubes on large and small particles of nickel. Although the methane dissolution rate of larger-sized nickel particles is low, sufficient carbon atoms can be generated to provide the need for carbon growth on the step edge, resulting in the growth of carbon nanotubes. On the contrary, due to the rapid rate of methane cracking on small-sized nickel particles, a large number of carbon growths at the pre-existing step sites, forming an encapsulation carbon, and inhibiting the growth of the new graphite layer

course of the reaction, indicating lower catalytic stability. The reduced catalytic stability of Fe/La_2O_3 was attributed to the encapsulation of metallic iron by carbon deposited on the catalyst. The structural characterization revealed the presence of different phases in the catalysts. The fresh Fe/CeO_2 catalyst contained CeO_2 and Fe_2O_3 phases, while the fresh Fe/La_2O_3 catalyst had $La(OH)_3$, Fe_2O_3, and $LaFeO_3$ phases. However, the reduced samples of both catalysts predominantly contained cerium and lanthanum orthoferrites. The study also observed the deposition of multi-walled carbon nanotubes on the catalysts, with different shapes depending on the support material. Spiral-shaped multi-walled carbon nanotubes with a double helical-shaped chain-like structure were formed on the Fe/La_2O_3 catalyst, which is rarely observed in methane decomposition. The nanocarbon deposited on the Fe/CeO_2 catalyst exhibited high crystallinity and graphitization. Overall, the study provides valuable insights for the development of efficient catalysts for CO*x*-free hydrogen production.

The addition of yttria (Y_2O_3) to the iron catalyst was found to increase its specific area, and thus, the performance and stability of the catalyst were maintained at higher temperatures. In this context, Karaismailoglu et al. (2020) investigated the catalytic methane decomposition using Fe-based catalysts and explored the effect of the addition of yttria on the catalyst's activity, performance, and stability. The Fe-based catalysts were prepared using the sol–gel method, and different samples with varying $Fe_2O_3/Y_2O_3/Al_2O_3$ ratios were analyzed. The experimental results showed that the addition of yttria to the iron oxide catalyst significantly increased its catalytic activity and stability. At temperatures of 750 °C and 800 °C, the methane conversions achieved with Fe_2O_3/Y_2O_3 and $Fe_2O_3/Y_2O_3/Al_2O_3$ catalysts were 29% and 4%, respectively. This indicates that the Fe-based catalysts are effective for methane decomposition, and the addition of yttria further enhances their performance.

Moreover, the characterization analyses of the catalysts revealed that the addition of yttria increased the specific area of the catalyst. This increase in specific areas contributed to the improved performance and stability of the catalyst, even at higher temperatures. The presence of yttria also prevented the formation of a garnet-type crystal structure, which could reduce the catalytic activity. Overall, the study demonstrates that Fe-based catalysts, especially those with yttria addition, are promising for CO*x*-free hydrogen generation through catalytic methane decomposition. The addition of yttria enhances the specific area of the catalyst and maintains its performance and stability, making it suitable for high-temperature applications. These findings contribute to the development of efficient catalysts for hydrogen production from methane, which is crucial for clean and renewable energy systems.

The utilization of Fe-based catalysts in methane decomposition was mainly for the generation of high-value, thin-walled carbon nanomaterial (Li et al. 2011). Awadallah et al. (2017b) successfully synthesized high-quality, few-layered graphene nano-platelets via catalytic chemical vapor deposition of methane using unsupported metal oxides, such as iron, cobalt, and nickel metallic sheets. The results showed that the unsupported metallic catalysts, particularly nickel, exhibited efficient catalytic growth activity for graphene nano-platelets. The unsupported nickel catalyst yielded 254 wt% of graphene nano-platelets, which was higher compared to the other catalysts. The reduction of the metal catalysts resulted in the formation of polycrystalline metallic sheets, which promoted the growth of graphene nano-platelets on their surfaces. The transmission electron microscopy images confirmed the formation of zero-valent metallic sheets after the complete reduction of the metal oxides. Raman spectroscopy and transmission electron microscopy analysis revealed that the synthesized graphene nano-platelets had a few layers, high crystallinity, and good graphitization.

Furthermore, the as-grown graphene nano-platelets exhibited significantly higher thermal stability in an air atmosphere compared to other synthesis methods. The study highlights the importance of zero-valent metallic sheets in enhancing the growth of graphene nano-platelets. The unsupported metallic catalysts, particularly nickel, demonstrated superior catalytic activity, resulting in high-quality graphene nano-platelets. These findings contribute to the understanding of graphene synthesis and pave the way for large-scale production of graphene nano-platelets with potential applications in various fields. It was found that the formation of zero-valent metallic sheets enhances the growth of graphene nano-platelets, and their mechanism is illustrated in Fig. 3.

Similarly, the formation of different carbon nanomaterials over Fe-based catalyst has been modeled using density functional theory (DFT) and experimental results. In this context, Zhou et al. (2017) presented a study on the synthesis and characterization of iron catalysts for methane decomposition to produce hydrogen and carbon nanomaterials. The authors investigated the activity of fused 65 wt% and impregnated 20 wt% iron catalysts with different additives. They found that the Fe–Al_2O_3 combination showed the best catalytic activity. The formation of carbon nanotubes was speculated to be facilitated by the exposure of Fe^0 on Al_2O_3. The optimized temperature for hydrogen pre-reduction and high activity was determined to be 750 °C. In addition, density functional theory was used to propose a reaction mechanism over iron catalysts, explaining the formation of graphite from the decomposition of unstable supersaturated iron carbides. The study also proposed a carbon deposition model to explain the formation of different carbon nanomaterials.

Overall, the study contributes to the understanding of iron catalysts for methane decomposition and provides insights into the formation of carbon nanomaterials. The combination of experimental results and density functional theory modeling enhances the understanding of the catalytic process and can guide future research in the development of efficient Fe-based catalysts for hydrogen production and carbon nanomaterial synthesis. Therefore, Fe-based catalysts drive the commercialization of catalytic methane decomposition, utilizing high-value carbon by-products to offset hydrogen production costs and increase revenue (Qian et al. 2020).

Co-based has also been studied for catalytic decomposition of methane and showed high stability at higher temperatures (Awadallah et al. 2018; Awadallah et al. 2016a; Dasireddy and Likozar 2017; Silva et al. 2016). The formation of Co_3O_4 contributed to the catalytic effect and durability of the Co-based catalyst in catalytic methane decomposition (Awadallah and Aboul-Enein 2015). The nature of support also affects the Co-based catalytic performance and its longevity (Silva et al. 2016; Awadallah et al. 2016a).

A study conducted by Al Mesfer et al. (2021) discussed the synthesis, evaluation, and kinetic assessment of a Co-based catalyst for enhancing the catalytic methane decomposition for hydrogen production. The researchers developed $Co/TiO_2–Al_2O_3$ catalysts with different cobalt loadings (10%, 30%, and 50%) using an ultrasound-assisted wet impregnation method. The catalysts were characterized using various techniques, and their activity was evaluated at 600 °C and 1 bar of pressure. The kinetic experiments for the 50% cobalt catalyst were conducted in the temperature range of 550–650 °C by varying the methane partial pressure. The results showed that the prepared catalysts exhibited good textural properties and high activity, with the activity and stability being directly related to the cobalt metal loading. The power-law model, which assumed a nonlinear dependency of reactant partial pressure on the methane decomposition rates, satisfactorily fits the experimental data. The apparent reaction order was determined to be 2.46, and the activation energy was calculated as 65.16 kJ/mol. The improved wet impregnation method successfully synthesized cobalt nanoparticles under 25 nm at a metal loading of 50%. The Co-based catalysts demonstrated promising performance in the catalytic methane decomposition reaction, providing high hydrogen production rates and generating solid carbon. The use of cobalt as the active metal allowed for the acceptance of electrons from methane and the activation of the C–H bond. The results also highlighted the importance of the catalyst support material, as mixed oxide supports such as $Al_2O_3–TiO_2$ showed better metal–support interaction and higher metal dispersion, leading to improved catalytic activity and stability.

In conclusion, the investigation into monometallic catalysts, particularly those based on nickel, iron, and cobalt, for catalytic methane decomposition presents a multifaceted understanding of their catalytic activity, stability, and potential applications. Ni-based catalysts have been extensively studied and widely utilized in catalytic methane decomposition processes due to their high catalytic activity, with significant research focusing on optimizing their performance through various synthesis methods and support materials. Studies have demonstrated the effectiveness of nickel catalysts, especially when supported on materials such as alumina, yttria, or mesoporous nanocrystalline gamma alumina, in promoting methane conversion to CO*x*-free hydrogen and valuable carbon nanomaterials. Similarly, Fe-based catalysts have emerged as a promising alternative, showcasing good catalytic activity and stability, particularly at higher operating temperatures. The addition of yttria has been found to enhance the performance and stability of iron catalysts, making them suitable for harsh conditions encountered in methane decomposition processes.

Additionally, iron catalysts have shown potential for the generation of high-value carbon nanomaterials, further highlighting their versatility in catalytic methane decomposition applications. While Co-based catalysts have also demonstrated high stability at elevated temperatures and have been studied for methane decomposition, their utilization is limited due to cost and toxicity concerns compared to Ni- and Fe-based counterparts. Overall, the research findings underscore the importance of catalyst selection, synthesis methods, and support materials in optimizing the efficiency and stability of catalysts for methane decomposition. Further exploration into catalyst modification and understanding the underlying mechanisms governing catalytic activity will be crucial for advancing catalytic methane decomposition technology toward sustainable and efficient hydrogen production while also addressing environmental concerns associated with carbon emissions.

Bimetallic and trimetallic catalysts

The use of multiple metals indicated the starting point of the second generation of industrial catalysts, overcoming deactivation by coke deposition. Ni-based mono-, bi-, and tri-metallic over alumina support have been tested for methane decomposition at 675 °C and 750 °C. Figure 4 shows that among the tested catalysts, the bimetallic and trimetallic catalysts had better activity and stability. The decrease in methane conversion was mainly due to the formation of encapsulating carbon on the surface of active sites, which could hinder the access of reactants to the active sites. The addition of iron to the nickel catalyst increased catalytic stability by increasing the carbon diffusion rate and preventing the formation of encapsulating carbon (Bayat et al. 2016b). On the other hand, the addition of copper could improve the

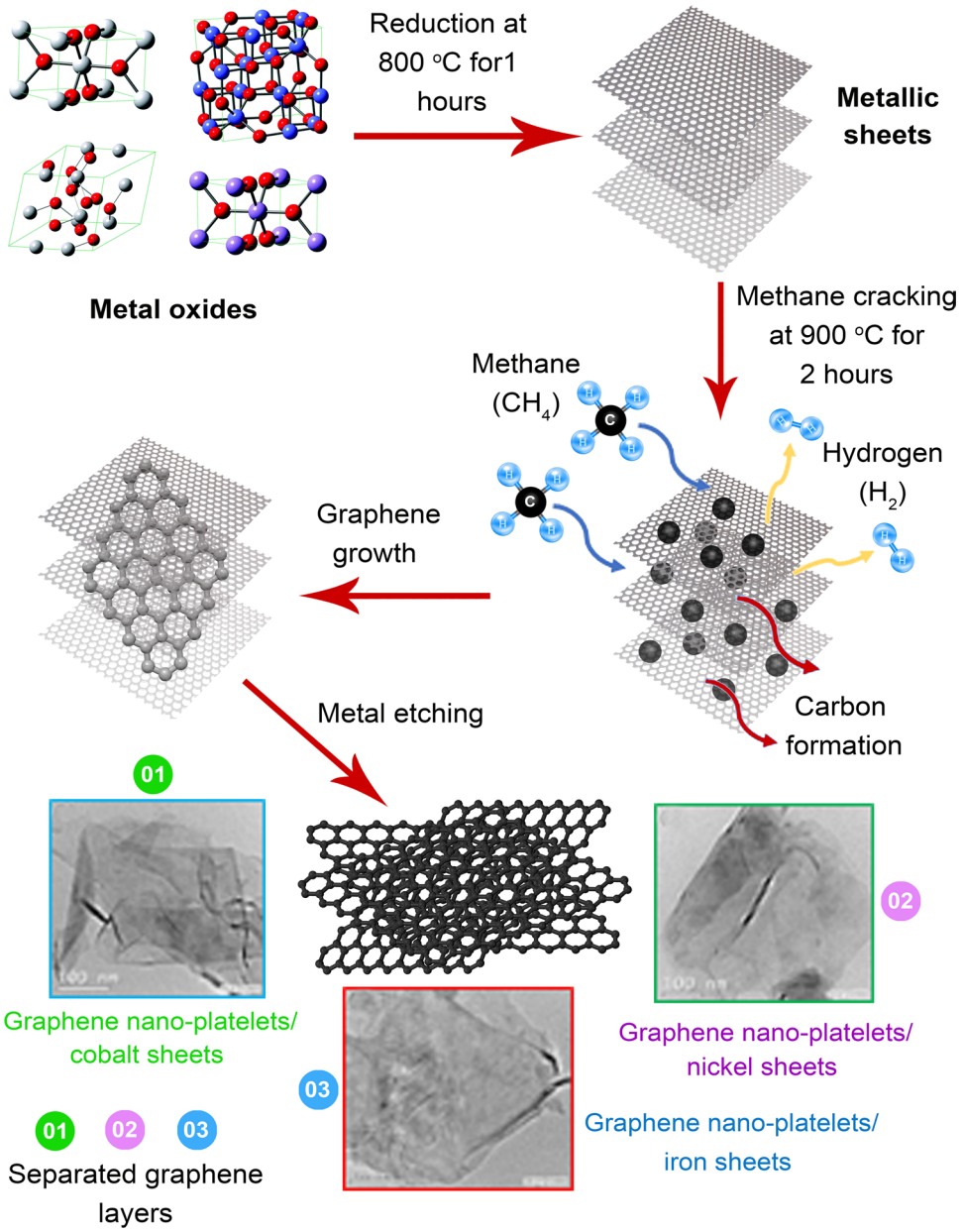

Fig. 3 Growth of graphene nano-platelets over the surface of reduced metallic sheets. The crystallinity and morphological structure of the reduced metallic sheet catalysts significantly influence both the number of graphitic layers and the graphene yield. As shown, the process involves the catalytic decomposition of a carbon-containing precursor on the surface of the metallic sheet, leading to the formation and growth of graphene nano-platelets. The size and orientation of the metallic sheets play a crucial role in dictating the morphology and quality of the resulting graphene layers. Understanding this mechanism is essential for optimizing graphene production processes and tailoring the properties of graphene nano-platelets for various applications ranging from electronics to energy storage

catalytic activity by enhancing the adsorption of methane on the surface of the catalyst.

In this context, Bayat et al. (2016c) investigated the catalytic performance of Ni–Fe–Cu/Al_2O_3 catalysts for the production of CO*x*-free hydrogen and carbon nanofibers through methane thermocatalytic decomposition. The study focuses on the effect of adding iron and copper as promoters to a nickel catalyst and their impact on the catalytic activity. The results showed that the addition of iron or copper to the nickel catalyst improved its catalytic performance. The presence of iron enhanced the carbon diffusion rate and prevented the formation of encapsulating carbon, leading to improved catalytic activity. However, it also decreased the reducibility of the nickel catalyst. On the other hand, copper increased methane adsorption and improved both the reducibility and nickel dispersion on the catalyst surface. Copper's high affinity with the graphite structure hindered the generation of encapsulating carbon on the nickel surface and prevented catalyst deactivation. The study found significant improvement in the catalytic performance of the promoted catalysts at temperatures higher than 700 °C. The regeneration studies of Ni–Fe/Al_2O_3 demonstrated that the catalyst could be reused up to 9 times (Fakeeha et al. 2018b). The addition of a small amount of oxygen (O_2) as a regenerative agent enhanced methane conversion, hydrogen yield, and catalyst stability.

Fe–Co/Al_2O_3 catalysts were synthesized and studied to produce hydrogen and multi-wall carbon nanotubes (Torres

et al. 2020). Fe–Co/Al_2O_3 catalysts produced higher carbon formations and longer stability at low temperatures (less than or equal to700 °C) by inhibiting the formation of Fe_3C during catalytic methane decomposition in non-doped catalysts. When the Fe_3C phase was found in the catalyst, it resulted in shorter multi-walled carbon nanotubes and higher production of the bamboo type due to its slower carbon diffusion than a-Fe (Torres et al. 2020).

Copper is being used as a promoter of Ni-based catalysts (Torres et al. 2018a; Awad et al. 2019; Cazaña et al. 2018; Li et al. 2017; Li et al. 2016). The 50%Ni–15%Cu/Al_2O_3 catalyst resulted in a 75% methane conversion at 750 °C for 6 h of transmission electron microscopy image demonstrated that graphene carbon, carbon nanofiber, and multiwall carbon nanofiber were encapsulated on the surface of a 50%Ni–15%Cu/Al_2O_3 matrix (Awad et al. 2019). Another investigation found that the Ni–Cu/SiO_2 catalyst showed catalytic stability at the temperature range of 500–750 °C, and the deactivated Ni–Cu/SiO_2 catalyst has recovered its performance due to the production of disordered carbon (Li et al. 2017). Moreover, copper doping on Ni-based catalyst resulted in $Ni_{(x)}Cu_{(1-x)}$ alloys with a larger lattice constant, allowing carbon diffusion to the particle. It enhanced the formation of denser carbon nanofilaments as well as increased the carbon formation rate (Torres et al. 2018a).

The incorporation of zinc in minor quantities alongside transition metals led to a decrease in carbon accumulation and enhanced the longevity of the catalyst. Saraswat and Pant (2011) investigated the impact of incorporating 5% zinc into a catalyst comprising 50% nickel and 50% copper supported on MCM-22, revealing that the addition of 5% zinc alongside 50% copper improved the catalyst's surface area. The catalytic efficiency was enhanced by introducing the zinc promoter alongside nickel and copper metals. The results indicate that the highest methane conversion achieved was 85%, with a carbon yield of 9.47%. The methane conversion increased with an increase in reaction temperature up to 750 °C and decreased at higher temperatures. The study highlights the potential of the thermocatalytic decomposition of methane as an eco-friendly route for producing CO*x*-free hydrogen and carbon nanotubes.

Other efforts to improve the effectiveness of catalytic methane decomposition catalysts used noble metals as promoters, such as platinum (Pudukudy et al. 2018), palladium (Bayat et al. 2016a) (Rategarpanah et al. 2018), ruthenium (Harun et al. 2020), manganese (Wang et al. 2020; Fakeeha et al. 2018b), and molybdenum (Awadallah et al. 2013a). This property of each metal improves the catalyst stability, which could increase lifetime. A synergetic effect of platinum promoter on 20%Ni/CeO_2 increased the activity and stability of the catalyst (Pudukudy et al. 2018). Carbon nanotubes with hollow channels formed over the Ni/CeO_2 catalyst were found to be more homogenous than those deposited on Pt-promoted catalysts. Ni–Pd/Al_2O_3 was synthesized by

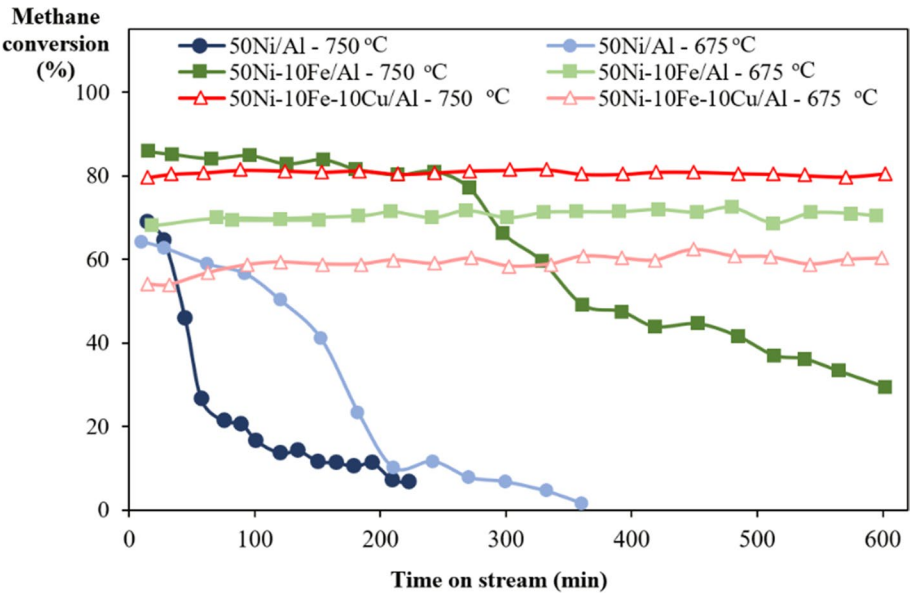

Fig. 4 Catalytic performance of mono-, bi-, and tri-metallic nickel-based catalyst on alumina support at different temperatures of 675 °C and 750 °C. The promotional effect of iron and copper for nickel catalyst in methane decomposition was observed due to the increasing carbon diffusion rate, enhancing methane adsorption, and preventing the formation of encapsulating carbon. Due to the endothermic nature of the methane decomposition reaction, the increase in temperature improved the initial methane conversion. However, the methane conversion and catalyst lifetime were reduced with excessively increasing reaction temperature because of a mismatch between the rates of carbon formation and migration (Modified from Bayat et al. 2016a, Bayat et al. 2016b)

the sol–gel method, and Ni–Pd alloy was created, leading to high catalytic activity for catalytic methane decomposition reaction (Bayat et al. 2016a). However, increasing the palladium content reduced the catalytic activity, which the reduction in surface area and particle agglomeration can explain.

Ni–Mo/Al_2O_3 catalyst has also been experimentally investigated for catalytic methane decomposition reaction (Awadallah et al. 2013b). The addition of molybdenum with other metals in bimetallic catalysts assisted the methane conversion and carbon nanotube bundle formation. The reduction of metal oxides to molybdenum carbides played an important role in catalyzing methane decomposition. The presence of molybdenum in a bimetallic catalyst could improve the stabilization and dispersion of nickel particles and give an intermediate-strength metal–support interaction; thus, the metal sintering was inhibited (Awadallah et al. 2013a).

In summary, the exploration of bimetallic and trimetallic catalysts for methane decomposition marks a significant advancement in industrial catalysis, overcoming challenges like coke deposition. Tests on Ni-based mono-, bi-, and trimetallic catalysts showed superior activity and stability in bimetallic and trimetallic configurations. The addition of iron enhanced catalytic stability by increasing carbon diffusion rates, while copper improved activity by enhancing methane adsorption. Studies revealed significant performance enhancements at temperatures above 700 °C. Regeneration studies demonstrated catalyst reusability, while Fe–Co/Al_2O_3 catalysts exhibited enhanced stability at lower temperatures by inhibiting Fe_3C formation. Copper-promoted Ni-based catalysts showed promising methane conversion rates, and the incorporation of zinc alongside transition metals reduced carbon accumulation. These findings underscore the potential of thermocatalytic methane decomposition for eco-friendly hydrogen and carbon nanotube production. Additionally, noble metal promoters such as platinum, palladium, and molybdenum further improved catalyst stability, highlighting diverse avenues for enhancing catalytic methane decomposition.

Carbon-based catalysts

Metal-based catalysts could result in a high initial hydrogen production and methane conversion; however, the activity of metal catalysts gradually decreases with time due to the deposition of coke on the surface of the catalyst, which becomes the main obstacle of metal-based catalysts. To fairly overcome this drawback, carbon catalysts, both as catalysts and support, were developed and investigated by many scholars. A carbon catalyst offers several advantages, such as good catalytic stability and performance, relatively cheapness, resistance to sulfur poisoning, and material tolerance at high temperatures (Zhang et al. 2017). Moreover, the deposited carbon nanomaterial over the surface of the catalyst was reported to help the catalytic activity up to a particular limit (Srilatha et al. 2016). However, carbon-based catalysts may also generate undesired by-products, i.e., larger hydrocarbons, which could reduce the catalyst activity, hydrogen yield, and methane conversion. The deposition of graphitic carbon on a carbon catalyst could block the active site. However, if the metal is mixed with the carbon materials, the deposition of filamentous carbon on the catalyst may aid in boosting hydrogen yield and improve methane conversion, improving overall process efficiency (Bai et al. 2007).

As the catalyst for the catalytic methane decomposition process, many kinds of carbon and metal–carbon compounds have been utilized, such as wood char (Dufour et al. 2008), biochar (Patel et al. 2020), activated biochar (Harun et al. 2020), graphite (Guil-Lopez et al. 2011), activated carbon (Harun et al. 2020; Pinilla et al. 2007), carbon black (Liu et al. 2018), ordered mesopores carbon (Shilapuram et al. 2014), and multi-wall nanotubes catalyst (Guil-Lopez et al. 2011). Table 3 shows the development and modification of carbon-based catalysts to improve their activity performance.

Activated carbon and carbon black are the most often utilized carbon-based catalysts due to their higher activity and greater stability. The catalytic performance of activated carbon and carbon black has been compared (Liu et al. 2018; Yang et al. 2020). The results indicated that the deactivation behavior of the activated carbon and carbon black differed with reaction time. The deposited carbon on the catalyst surface varies in form, orientation, and chemical structure. The outwardly developing cone-like graphene layers and tubular-shaped nanostructures contribute to the catalyst's porosity and activity. The uneven, cross-linking graphene layers of activated carbon and the spherical bent graphene layers of carbon black may be responsible for the disparity in carbon deposition (Liu et al. 2018). Activated carbon had a high initial methane conversion but was easily deactivated, whereas carbon black had a lower initial methane conversion but improved long-term stability (Yang et al. 2020), as depicted in Fig. 5.

On the other hand, the catalytic activity of biochar and activated char formed is determined by the physiochemical properties of the catalyst and the textural morphology of the deposited carbon (Patel et al. 2020). Interestingly, the growth of crystalline carbon deposition on the original catalyst may act as a fresh catalyst for catalytic methane decomposition reactions. Furthermore, the amorphous carbon catalyst exhibits better catalytic performance than the structure form (Muradov 2001). To further elevate the advantages of carbon-based catalysts, ordered mesoporous structure carbon has been synthesized to enhance the catalyst activity (Shilapuram et al. 2014). The synthesis of ordered mesoporous structure carbon nano-rods (CMK-3)

and cubic ordered mesoporous structure carbide-derived carbon (DUT-19) is displayed in Fig. 6. Cubic ordered mesoporous structure carbide-derived carbon catalytically performed better than ordered mesoporous structure carbon nano-rods due to its larger surface area, higher pore volume, and lower threshold temperature. The results revealed that carbon deposition on the catalyst induced deactivation of the catalyst with considerable surface aggregation with block porous structures. The regeneration of a deactivated active carbon catalyst utilizing carbon dioxide as an activating agent was also investigated under various regeneration settings. Finally, following three repeated deactivation (850 °C, 480 min) and regeneration cycles (925 °C, 120 min), the catalytic activity of the catalyst may be completely recovered (Pinilla et al. 2007), as presented in Fig. 7.

Recently, researchers studied the possibility of enhancing the performance of carbon catalysts by adding active metals (Harun et al. 2020; Bai et al. 2007; Wang et al. 2017). Robust Ni/carbon was successfully synthesized by selective steam gasification of pine sawdust. Highly dispersed Ni/carbon was directly applied for in situ catalytic methane decomposition, which provides stable methane conversion (greater than 90%) at 850 °C for 600 min (Zhang et al. 2018). The carbon microfibers synthesized by needle-less electrospinning were used as catalyst support and impregnated with nickel, copper, and cobalt metals, and transition metal phosphite was tested at 800 °C for methane decomposition. The morphology, heat treatment, and type and content of incorporated transition metals and metal phosphides play a vital role in controlling parameters in the catalytic decomposition of methane (Sisáková et al. 2019).

Harun et al. (2020) compared the performance of ruthenium–activated carbon (Ru–AC), activated carbon, and activated biochar catalysts for the catalytic decomposition of methane at 800 °C. As shown in Fig. 8, activated biochar and ruthenium–activated carbon showed higher hydrogen production as compared to activated carbon after 60 h of reaction time; ruthenium–activated carbon and activated biochar still exhibited 21% and 51% of methane conversion, respectively. The high surface area of activated biochar (3256 m^2/g) plays a more crucial role in the catalytic activity than that of ruthenium–activated carbon (693 m^2/g) and activated carbon (776 m^2/g). But the surface area of activated biochar was decreased to 1893 m^2/g, after 8 h of reaction. Surprisingly, after 50 h of reaction, activated biochar still had a higher surface area (746 m^2/g) than fresh Ru–AC (693 m^2/g). They concluded that the initial high surface area and the carbon nanotube growth in activated biochar played an important role in stability for the long reaction run. The interaction of metal support plays a crucial role in carbon nanotubes growth and catalyst deactivation. The growth of carbon nanotubes could separate ruthenium from activated carbon, and ruthenium particles were deposited by carbon, leading to deactivation after a long run.

Carbonization of coal with ferric nitrate ($Fe(NO_3)_3$) addition under potassium hydroxide (KOH) activation was used to directly produce Fe-doped carbon catalysts. The carbonization at low temperatures resulted in the high initial conversion of methane, whereas active sites of Fe-doped carbon catalysts catalyst generated at higher temperatures were mostly created from metal (Fe) particles, resulting in improved stability but reduced initial catalytic performance (Wang et al. 2017).

From the literature survey, it can be briefly concluded that carbon-based catalyst offers several merits over metal catalysts due to their availability, durability, and low cost. In addition, the carbon produced during the process could catalyze the reaction, eliminating the need for an additional catalyst. The separation of the carbon product from the catalyst may not be necessary. Unfortunately, the lower methane conversion and hydrogen yield of carbon catalysts limit the practical use of this catalyst in the catalytic methane decomposition process. Furthermore, carbon catalysts remain a significant problem, particularly because the reaction mechanism must be defined in order to increase catalytic performance further. In-depth, the relationship between carbon catalyst features such as surface area, porosity, structural functionality, and its role in reaction processes remains unknown.

Furthermore, it appears that regeneration of the deactivated carbon catalyst is required for the continuing catalytic breakdown of methane. If regenerative agents such as oxygen, air, or steam are utilized during the regeneration process, both the deposited carbon and the original carbon catalyst may be gasified or burned. Doping active metals such as nickel, iron, and cobalt are believed to enhance catalytic activity; nevertheless, deactivation of carbon-supported catalysts is inevitable due to catalyst encapsulation by carbon deposition and/or metal carbide formation.

In summary, carbon-based catalysts offer stability and performance advantages over metal-based ones but can generate undesired by-products. They include various forms such as activated carbon, carbon black, and biochar. The morphology and properties of the deposited carbon significantly influence catalyst performance. Adding active metals such as nickel and cobalt can enhance catalytic activity. Regeneration of deactivated carbon catalysts is crucial for sustained methane breakdown. However, deactivation due to carbon deposition and metal carbide formation remains a challenge for carbon-supported catalysts.

Role of the support

The catalyst support plays a role in the catalytic activity and metal–support interaction. Suitable support with proper

Table 3 Characterization and performance evaluation of carbon-based catalysts for catalytic methane decomposition to hydrogen

Catalyst	Synthesis strategy	Temperature (°C)	Reaction time (minute)	Hydrogen yield (%)	Methane conversion (%)	Catalyst performance remarks	References
CG Norit	Commercially available CG Norit (granular activated carbon produced by chemical activation using the phosphoric acid process)	850	480	75	60	The surface properties of the catalyst decreased after continuous deactivation and regeneration cycles, but graphite-like carbon was resistant to gasification, with the first CG Norit catalyst gasified after three cycles	Pinilla et al. (2007)
Activated carbon	Commercially available activated carbon (coconut shell-based)	900	350	96.5	Not available	The activated carbon catalyst demonstrated excellent catalytic performance but rapidly deactivated after 6 h due to dense amorphous carbon deposition on its surface, causing loss of surface area and porosity	Liu et al. (2018)
Carbon black	Commercially available carbon black	900	350	30.5	Not available	Carbon black's low activity was maintained after the reaction due to its porous morphology and outward carbon growth on the catalyst surface. This stable performance preserves carbon black's surface properties	Liu et al. (2018)
Activated biochar	Activated biochar and heat-treated biochar are produced from Douglas-fir biochar	800	480	Not available	69	Activated biochar derived from Douglas-fir showed comparatively stable methane conversion. The high surface area and its microporosity caused resistance against rapid deactivation. The formation of carbon nanotubes contributed to the lifetime of activated biochar	Harun et al. (2020)
Ni/carbon	Pine sawdust pre-impregnated with nickel	850	600	Not available	90	Highly dispersed and robust nickel doped on carbon catalysts (Ni/carbon) can be in situ produced by steam gasification of pine sawdust. Gasification conditions affected the activity of synthesized catalysts	Zhang et al. (2018)
Ru–activated carbon	Commercial activated carbon doped by 3 wt% ruthenium	800	480	Not available	73	The loading of ruthenium could reduce the reduction temperature of the catalyst. Ru–activated carbon had slightly higher dispersion, specific area, and smaller crystalline size than Ru-zeolite socony mobil-5 (Ru-ZSM-5), which contributed to the micropores, mesopores, and macropores	Harun et al. (2020)

Table 3 (continued)

Catalyst	Synthesis strategy	Temperature (°C)	Reaction time (minute)	Hydrogen yield (%)	Methane conversion (%)	Catalyst performance remarks	References
Fe–activated carbon	Activated carbon doped by 30 wt% iron	850	550	Not available	58	The amount of iron and carbonization temperature affected the textural properties of the catalyst. The specific surface area decreased with increasing iron amount but increased hydrogen output and methane conversion	Wang et al. (2017)

This table presents the synthesis strategies, reaction conditions, and performance evaluations of various carbon-based catalysts utilized in methane reforming processes. Each entry details the catalyst type, synthesis method, reaction temperature, reaction time, hydrogen yield percentage, methane conversion percentage, and specific catalyst performance remarks. Commercially available activated carbons, carbon blacks, and activated biochar are among the catalysts evaluated, along with nickel- and ruthenium-doped carbon catalysts. Insights into catalyst stability, activity, and surface properties are provided, offering valuable information for further research and development in catalytic methane decomposition

preparation techniques could enhance the catalytic performance. The excellent support should have favorable properties such as a high surface area, coke resistance, thermal stability, and mechanical resistance. The high surface area will help to create strong metal–support interaction, leading to enhanced dispersion of metal active sites over the surface of support materials. Salam and Abdullah (2017) revealed that the acidity of the support would also help the catalyst to become thermally stable from sintering and coke deposition due to the appropriate metal and support interaction. Metal oxide compounds such as Al_2O_3, SiO_2, MgO, TiO_2, La_2O_3, CeO_2, ZrO_2, and their combination were used as catalyst support (Ahmed et al. 2016; Awadallah et al. 2018; Torres et al. 2018b; Németh et al. 2019; Srilatha et al. 2018; Al -Fatesh et al. 2020; Rastegarpanah et al. 2017a). Furthermore, the utilization of carbon-based material as a support has also been studied (Harun et al. 2020; Wang et al. 2017).

Ni-based catalysts on different support materials (SiO_2, TiO_2, graphite, ZrO_2, MgO, Al_2O_3, $SiO_2{\cdot}Al_2O_3$, and $MgO{\cdot}SiO_2$) have been catalytically tested (Takenaka et al. 2001). They reported that nickel catalysts on SiO_2, TiO_2, and graphite support exhibited high activities and long life of reaction time, while the remaining supports were inactive for reaction due to fast deactivation. Interestingly, they reported that pore structures of the support materials play a key role in the catalytic lifetime. The silica support without pore structure resulted in the best catalytic activity and longest catalyst lifetime.

Chesnokov and Chichkan (2009) synthesized bimetallic and trimetallic supported on Al_2O_3 using mechanochemical activation for catalytic decomposition of methane. The results implied that the high dispersion of Al_2O_3 particles between the metals and their alloys reduced the contact between the metals, preventing the metal sintering. This contributed to the stability of the catalysts and their ability to operate at high temperatures. A similar finding was also reported where the metal particles of nickel and cobalt could be well-attached and distributed inside the Al_2O_3 support matrix after being treated at high temperatures (Gao et al. 2020a). However, a gradual deactivation of the catalyst was still observed with increasing reaction time due to the blockage of the active surface by produced carbon nanotubes.

The aerogel catalysts containing bimetallic transition metals supported on aerogel composite supports ($9Ni–1Co/Al_2O_3{\cdot}TiO_2$) were successfully synthesized and exhibited higher catalytic performance than single support ($9Ni–1Co/Al_2O_3$). The composite support could improve the metal–support interaction and enhance the dispersion of active metals, resulting in better catalytic activity and a lower deactivation rate of the catalyst (Gao et al. 2019a). The formation of nickel aluminate ($NiAl_2O_4$) spinel structure is suppressed with the addition of titanium dioxide (TiO_2), leading to an increase in catalytic activity

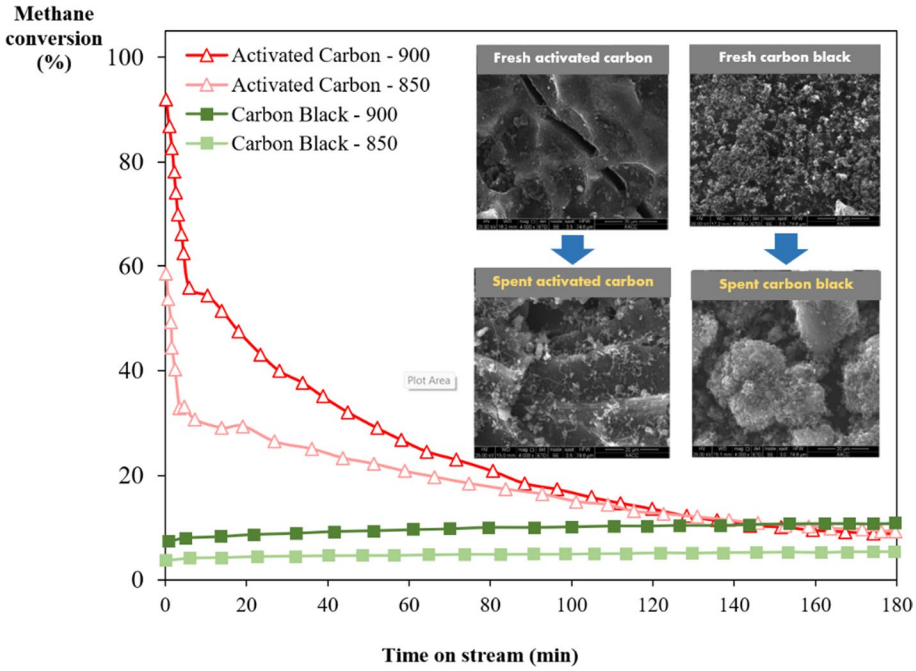

Fig. 5 Catalytic activity of activated carbon and carbon black catalyst at 850 °C and 900 °C; herein after denoted as activated carbon-850, activated carbon-900, carbon black-850, and carbon black-900. Activated carbon showed a high initial methane conversion, but it deactivated quickly. In contrast, carbon black has shown stable activity at lower methane conversion. The carbon formed on activated carbon was the most amorphous. Meanwhile, carbon black produces structured or more crystalline carbon (modified from Yang et al. 2020)

(Awadallah et al. 2014b). The strong metal–support interaction between nickel and TiO_2 was also reported to give a high dispersion of nickel particles on the surface of TiO_2 (Shen and Lua 2015).

The nature of support also affects the Co-based catalytic performance and its longevity in catalytic methane decomposition (Silva et al. 2016; Awadallah et al. 2016a). Various binary oxides (ZrO_2–MgO, ZrO_2–Al_2O_3, ZrO_2–La_2O_3, and ZrO_2–CeO_2) supported cobalt have been investigated (Awadallah et al. 2018). The results showed that the addition of secondary oxides to the zirconium dioxide (ZrO_2) support played a crucial role in the performance of the cobalt catalyst. Among the supported catalysts, Co/Zr–Mg exhibited the highest activity in terms of hydrogen yield. The moderate interaction between cobalt oxide and the magnesium oxide (MgO) support, leading to the formation of CoMgO*x* species, enhanced the dispersion of cobalt (II, III) oxide (Co_3O_4) and prevented its aggregation on the catalyst surface.

On the other hand, the Co/Zr–Si catalyst had the lowest activity due to the agglomeration of Co_3O_4 on the silicon dioxide (SiO_2) support. The researchers also observed that the deposited carbon on the spent catalysts mainly consisted of multi-walled carbon nanotubes. This finding is significant as it demonstrates the potential for the production of valuable carbon nanomaterials alongside hydrogen generation. Overall, the study highlights the importance of the support material in influencing the activity and stability of the cobalt catalyst for methane decomposition. The addition of secondary oxides to the ZrO_2 support can enhance the catalytic performance and prevent catalyst deactivation. These findings contribute to the development of efficient catalyst systems for CO*x*-free hydrogen production, which is crucial for clean energy applications. The findings revealed that metal–support interaction plays an important role in the performance of Co-based catalysts. However, due to cost and toxicity concerns, Ni- and Fe-based catalysts are more extensively utilized in methane decomposition than Co-based catalysts.

The addition of MgO to Al_2O_3 support has received great interest from many researchers due to its excellent properties, e.g., high melting point and high thermal and mechanical properties that can be used for catalyst supports. The mixed metal oxides called magnesium aluminate ($MgAl_2O_4$) spinel with mesoporous nanocrystalline, and high surface area can be prepared through co-precipitation, sol–gel, solid-state reaction (Rastegarpanah et al. 2017a). MgO is a popular catalyst support for carbon nanotube growth and deposition due to its high metal dispersion and carbon growth. It can be easily removed from deposited nanocarbons through normal acid treatment without damaging its structure or crystalline quality. Rastegarpanah et al. (2017b) investigated the effect of $MgAl_2O_4$ as a support for Ni-based catalyst on methane decomposition under various operating conditions. The finding showed that the mesoporous nanocrystalline structure of a catalyst with a high surface area was observed. However, with the increase in MgO/Al_2O_3, the surface area decreased while the average pore diameter increased.

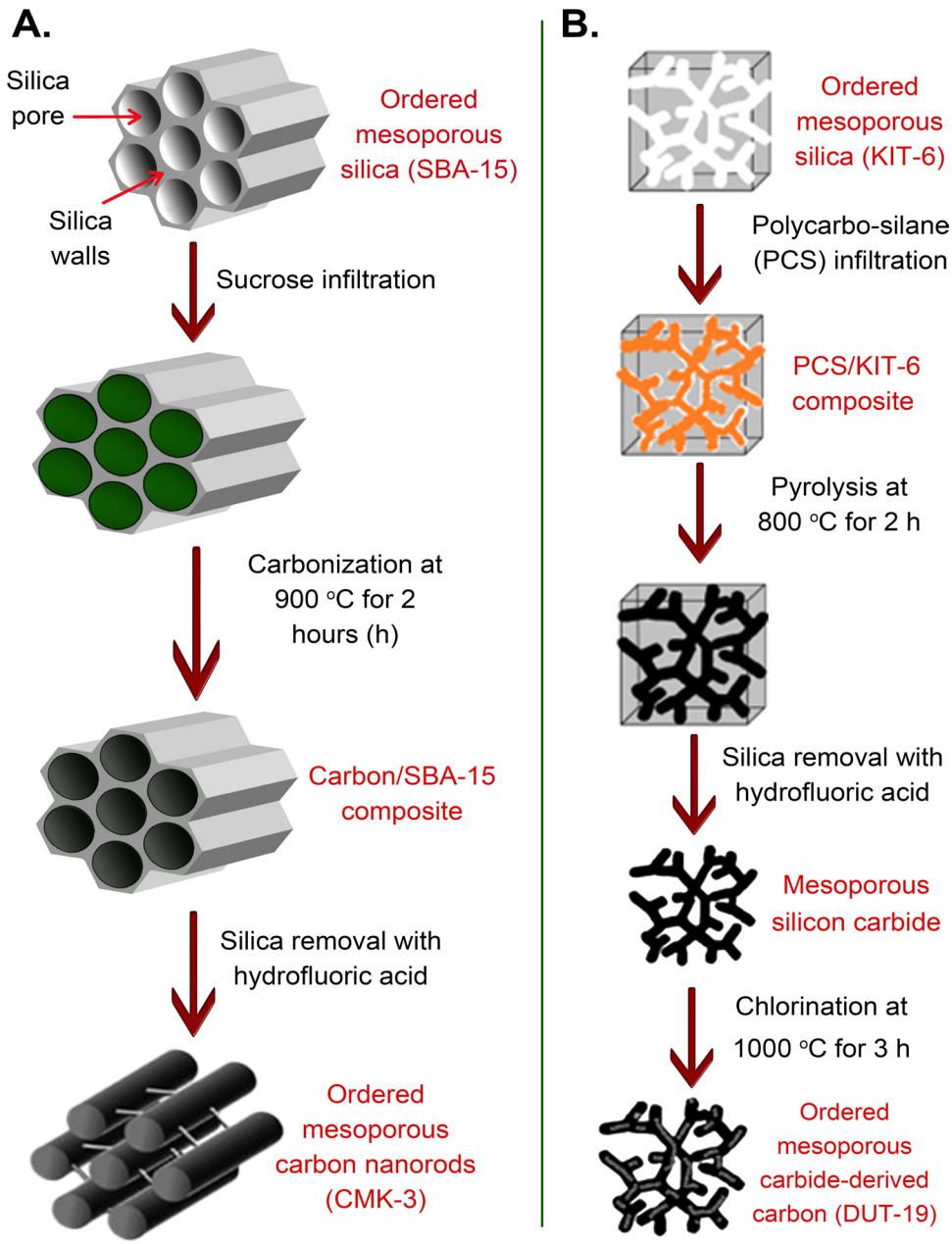

Fig. 6 Synthesis of **a** cubic ordered mesoporous structure carbide-derived carbon (DUT-19) and **b** ordered mesoporous structure carbon nano-rods (CMK-3). The mesoporous, carbonaceous catalysts cubic ordered mesoporous structure carbide-derived carbon and ordered mesoporous structure carbon nano-rods were tested for hydrogen and carbon formation via methane decomposition. The ordered mesoporous structure carbon nano-rods showed better catalytic activity than that of cubic ordered mesoporous structure carbide-derived carbon due to its higher pore volume. The carbon deposition on the outer surface and agglomeration of particles and/or carbon tubes contributed to the deactivation of the catalyst

In addition to acting as a catalyst, carbon-based materials are widely used as a support in heterogeneous catalysts. Carbon black and activated carbon are widely used for support due to their physicochemical properties, allowing for large surface areas and high porosity for active site dispersion. They are mainly derived from natural resources, even though a series of activation treatments are necessary to develop a desired property. But it still offers lower cost compared to conventional metal support. Nowadays, a wide range of new and advanced nanocarbon materials such as graphene, carbon nanotubes, fullerene, and their derivatives are being specially developed for many applications (Saha and Dutta 2022; Gamal et al. 2021). Carbon-based materials are recognized as the most promising direction to develop next-generation nano-engineered catalytic materials (Ampelli et al. 2014). Besides its advantages, carbon supports can be easily gasified or burned when the oxidants (air, oxygen, steam, and carbon dioxide) are used during catalyst regeneration. The role of carbon in catalysis mechanisms is still required in detail for the improvement of the catalytic activity. The role of support in the catalytic decomposition of methane is summarized in Table 4.

In summary, catalyst support greatly influences activity and stability. Suitable supports offer high surface area,

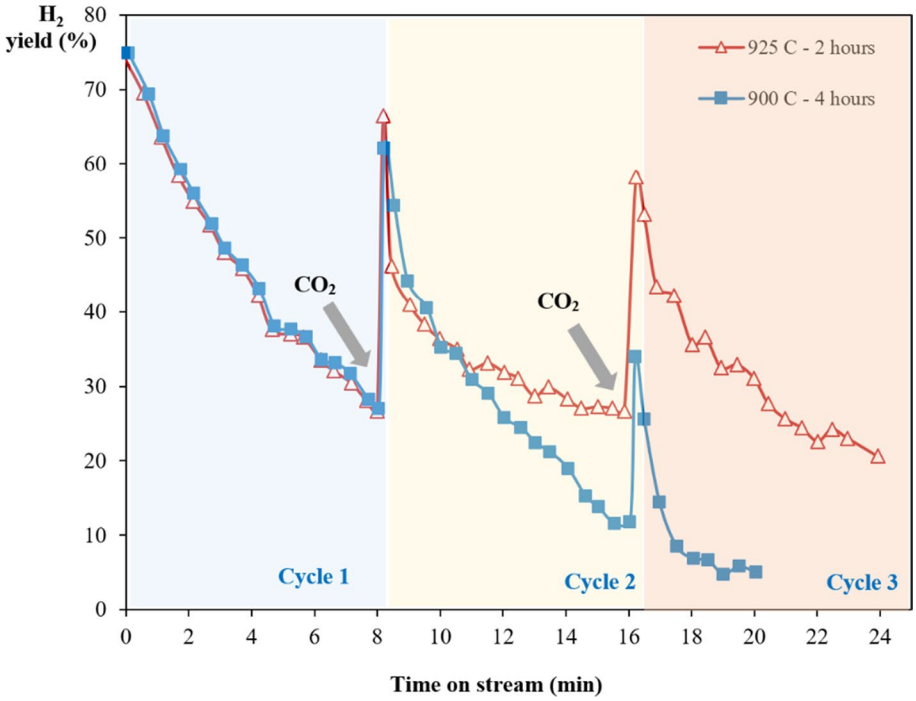

Fig. 7 The profile of hydrogen production was examined after regeneration cycles under various regeneration conditions, specifically at 900 °C for 4 h and 925 °C for 2 h. The investigation focused on the regeneration of a deactivated carbon-based catalyst using carbon dioxide as the regenerative agent. Throughout successive deactivation–regeneration cycles, a noticeable decline in the initial methane decomposition rate was observed. Concurrently, there was a gradual decrease in the textural properties of the catalyst, indicating changes in its structural characteristics over the regeneration cycles. These findings shed light on the dynamic behavior of the catalyst during the deactivation and regeneration processes, which is crucial for understanding and optimizing its long-term performance (modified from Pinilla et al. 2007)

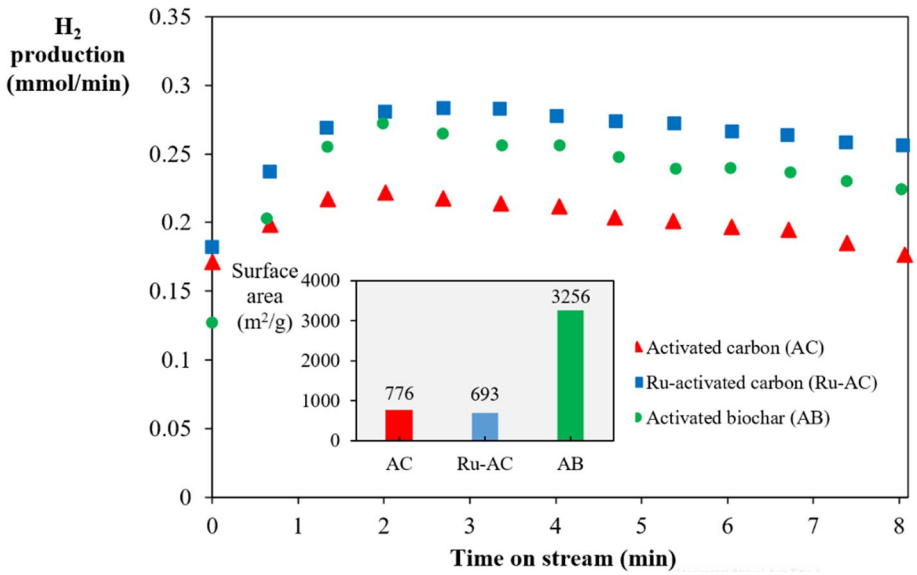

Fig. 8 Hydrogen production from catalytic methane decomposition using activated carbon (AC), Ru–activated carbon (Ru–AC), and activated biochar (AB) catalysts at 800 °C. The catalytic activity of activated biochar derived from Douglas-fir biomass was compared with commercial activated carbon and ruthenium-doped activated carbon. It is worth mentioning that surface area plays an important role in catalyst performance. A higher surface area provides higher space for methane to be absorbed on the surface of the catalyst (modified from Harun et al. 2020)

resistance to coke deposition, and thermal stability. Various compounds such as Al_2O_3, SiO_2, and MgO serve as effective supports. Carbon-based materials, including graphene and carbon nanotubes, also play a crucial role. Overall, support selection significantly impacts catalytic efficiency.

Catalyst deactivation mechanisms and reactivation pathways

Catalytic decomposition of methane catalyst deactivates largely due to high-temperature metal sintering and unavoidable co-product carbon formation. One of the most common challenges in the catalytic decomposition of methane is the deactivation of the catalyst during the reaction. Generally, during a catalytic process, the activity and product selectivity of a catalyst do not remain permanently intact. However, the extent of deactivation varies from one catalyst to another since some of the catalysts show rapid deactivation while others maintain their catalytic performance for as long as months. The factors behind catalyst deactivation include metal particle agglomeration, also known as sintering, and catalyst poisoning due to the presence of certain gas, such as hydrogen sulfide, carbon formation, also called coking, and attrition and/or mechanical degradation (Abbas and Daud 2009). Sintering, in general, involves metal particle enlargement or agglomeration at elevated temperatures, which leads to loss of the specific surface area available for reactant adsorption and subsequent activation. The following paragraphs highlight only two factors such as sintering and coking, leading to catalyst deactivation during the catalytic decomposition of methane.

Sintering

The higher reaction temperatures promote metal agglomeration and/or sintering that leads to catalyst activity loss since sintering is an irreversible deactivation pathway (Arku et al. 2018; Araújo et al. 2021; Eggenhuisen et al. 2013). A heterogeneous catalyst comprises active metal components and support material; hence, one can divide sintering into active metal sintering (AMS) and/or support sintering (SS). Active metal sintering indicates the perpetual growth of active metal particles into larger ones. Sintering involves two major mechanisms: (1) atomic migration, better known as Ostwald ripening, in which a particle is first released from a metal that is later taken by another neighboring particle; (2) particle migration, in which two metal particles traveling over the surface of a support bump into each other to form a larger metal particle. Particle migration dominates at lower temperatures, while higher temperatures facilitate atomic migration, in particular during long-term reactions (Gao et al. 2020b). Besides reaction time and temperature, catalyst composition, structure, and support morphology also play a role in defining the sintering. On the contrary, solid-state diffusion, grain boundary diffusion, and surface diffusion, as well as volatile molecule condensation and/or evaporation and phase transformation, are the factors affecting the sintering of support (Pham Minh et al. 2021). One of the examples of phase transformation with respect to temperature includes variation in alumina crystal phase from ?-phase to a-phase at elevated temperatures between 1000 and 1125 °C, leading to a sharp reduction in the specific surface area (Argyle and Bartholomew 2015).

Metal-based catalyst deactivation

Several studies have discussed catalyst deactivation with an aim to extend the lifetime of the catalyst during methane decomposition. These studies are mostly focused on discussing the parameters that influence deactivation, the stability period of the catalyst prior to its deactivation, and the time it takes a catalyst to deactivate completely. Table 4 clearly illustrates the catalytic deactivation behavior of numerous catalysts over time during the catalytic decomposition of methane. It also covers various parameters, such as the initial conversion of methane and/or yield of hydrogen, along with these values at time (t). The results provide insight into the loss of catalytic activity over time for different catalysts.

The by-product of methane decomposition comprises various forms of carbon with different chemical structures, including graphitic carbon, amorphous carbon, filamentous carbon, and carbon structure with a higher carbon/hydrogen ratio called polyaromatic carbon (Li et al. 2011). Table 5 depicts the influence of different catalysts, gas hourly space velocity (GHSV), and temperature on the amount and types of carbon produced by the catalytic decomposition of methane; as can be seen, different catalysts resulted in different amounts of deposited carbon. It has been agreed among the scientific community that the deposition of carbon over the surface of the catalyst is mainly accountable for catalytic deactivation (Zhang and Smith 2004).

In the first step, methane dissociatively adsorbs over the surface of the metal, followed by dissolution into products along with desorption of hydrogen. Subsequently, carbon adsorbed over the catalyst surface diffuses through the metal and precipitates at the rear-end of the metal, leading to the formation of filamentous carbon. However, during carbon growth, metal crystallites get separated, and these detached metal crystallites facilitate further growth of carbon filaments for a prolonged time before these crystallites are encapsulated with carbon and eventually get deactivated (Figueiredo 1982).

Scientists have also presented various other carbon growth mechanisms in the recent past. According to Baker et al. (1972), carbon growth comprises four basic steps, i.e., (a) the chemisorption of methane via C–H bond breakage at the front-end of a catalyst particle, (b) chemisorbed hydrogen accumulation into molecules and subsequent desorption into gaseous phase, (c) carbon diffusion through bulk of the catalyst from the front-end to the rear-end, and (d) formation of carbon nanomaterials via carbon nucleation

Table 4 Catalytic deactivation behavior of various catalysts over time during methane decomposition, along with parameters such as initial methane conversion and hydrogen yield at a time (*t*)

Catalyst	Support	Reaction conditions T (°C)/ GHSV(L/h g_{cat})	Initial Y_{H_2}/X_{CH_4} (%)	Y_{H_2}/X_{CH_4} (%) at time (t)	Time (*t*) (hour)	References
NiO	No support	800/4.5	45/Not available	49/Not available	6	Pudukudy et al. (2016)
Fe_2O_3	No support	800/4.5	36/Not available	46/Not available	6	Pudukudy et al. (2016)
Ni	Al_2O_3	650/42	Not available/79.2	Not available/68.7	1	Gao et al. (2019b)
Co	Al_2O_3	650/42	Not available/64.7	Not available/37.8	1	Gao et al. (2019b)
Ni	Zeolite Socony Mobil-5 (ZSM-5)	700/6	77/Not available	62/Not available	3	Awadallah et al. (2016b)
Ni	SiO_2	700/6	77/Not available	13/Not available	3	Awadallah et al. (2016b)
Ni	Santa Barbara Amorphous-15 (SBA-15)	700/9	46/Not available	39/Not available	7	Pudukudy et al. (2015)
Ni-Pd	Santa Barbara Amorphous-15 (SBA-15)	700/9	59/Not available	47/Not available	7	Pudukudy et al. (2015)
Fe	$WO_3{\cdot}ZrO_2$	800/4	49/46	41/39	4	Fakeeha et al. (2020)
Fe	$La_2O_3 + ZrO_2$	800/4	92/83	79/78	4	Fakeeha et al. (2020)
Fe–Ni	$La_2O_3 + ZrO_2$	800/4	91/92	92/93	4	Fakeeha et al. (2020)
Fe	$CeZrO_2$	700/6	83/85	33/36	2	Ramasubramanian et al. (2020)
Fe–Co	$CeZrO_2$	700/6	90/90	52/54	2	Ramasubramanian et al. (2020)
Fe–Mo	$CeZrO_2$	700/6	90/90	50/45	2	Ramasubramanian et al. (2020)
Co	SiO_2	700/6	80/Not available	38/Not available	7	Awadallah et al. (2016a)
Co	MgO	700/6	81.5/Not available	65/Not available	7	Awadallah et al. (2016a)
Co	Al_2O_3	700/6	81.5/Not available	90/Not available	7	Awadallah et al. (2016a)
Fe–Co	MgO	700/6	45/Not available	86/Not available	9.5	Awadallah et al. (2014a)
Ni	Al_2O_3–CeO_2	700/6	42/Not available	50/Not available	6.5	Ahmed et al. (2016)
Ni	Al_2O_3	700/6	39/Not available	47/Not available	6.5	Ahmed et al. (2016)
Ni	CeO_2	700/6	41/Not available	38/Not available	6.5	Ahmed et al. (2016)
Ni	Si–Al	700/6	79/Not available	32/Not available	6.5	Awadallah et al. (2013c)
Co	Si–Al	700/6	65/Not available	42/Not available	6.5	Awadallah et al. (2013c)
Ni–Co	$Al_2O_3{\cdot}TiO_2$	650/26.3	Not available/69.3.5	Not available/66.3	1	Gao et al. (2019a)
Ni–Co	$Al_2O_3{\cdot}TiO_2$ aerogel	650/26.3	Not available/72.5	Not available/72.5	1	Gao et al. (2019a)
Ni	HZSM-5/MCM-41	620/36	78/66	78/Not available	6	Alalga et al. (2021)
Ni	HZSM-5	620/36	74/60	74/Not available	6	Alalga et al. (2021)
Ni	MCM-41	620/36	71/55	72/Not available	6	Alalga et al. (2021)
CG Norit	No support	850/0.30	75/60	30/15	8	Pinilla et al. (2007)
Ni	Carbon	850/ Not available	Not available/80	Not available/90	10	Zhang et al. (2018)

The data sheds light on the evolution of catalytic activity over time for different catalysts, offering valuable insights into their performance dynamics. Results elucidate the loss of catalytic activity over time, which is crucial for understanding catalyst stability and informing future research in methane decomposition processes. T refers to temperature, GHSV refers to gas hourly space velocity, Y_{H_2} refers to hydrogen yield, and X_{CH_4} refers to methane conversion

at the rear-end of the catalyst. The same group of researchers have also proposed three-step carbon growth during the catalytic decomposition of methane. Initially, the adsorption and decomposition of hydrocarbons take place over the catalyst's active sites. In the next stage, carbon species dissolve through active metal from the hotter front-end face, which is exposed to the gaseous phase, to the cooler rear-end face and eventually carbon precipitates to form filamentous carbon. Ultimately, growing carbon encapsulates the catalyst's active sites, and hence, the growth rate is decreased. It can be inferred that the rate of catalyst deactivation is correlated with the rate of carbon diffusion. Hence, to maintain the activity of a catalyst, the rate of carbon diffusion needs to be higher than the rate of carbon growth, else carbon encapsulation of the catalyst leading to its deactivation is inevitable.

It has been reported that carbon formation is linearly proportional to the reaction temperature and has an inverse relationship with the partial pressure of methane (Villacampa et al. 2003). Catalysts may start to disintegrate at higher amounts of carbon formation. Furthermore, the factors affecting the catalytic activity with respect to carbon growth (Amin et al. 2011), include (a) stronger adsorption of the carbon on active sites covers the active sites and prevents the feed gas from approaching active sites; (b) active site gets completely encapsulated by carbon formed over the surface of the catalyst; (c) carbon negatively influences the textual properties of the catalyst by blocking the pores and eventually access of feed gas inside the pores; (d) can lead to disintegration of catalyst pellets associated with the formation of sturdy carbon filaments; and (e) carbon formation under extreme conditions can end up physically blocking the reactor tube.

The catalyst deactivation has also been found to be a function of the operating parameters such as partial pressure of reactant (methane) and product (hydrogen), operating temperature, and feed gas flow rates and/or gas hourly space velocities (Villacampa et al. 2003; Ermakova et al. 2000). The widely investigated role of operating temperature and feed gas flow rate has shown that these parameters are vital in affecting both the rate of methane decomposition and catalyst deactivation. At higher reaction temperatures, higher decomposition rates promote the rate of carbon nucleation. Hence, the rate of carbon nucleation is too fast for carbon diffusion to catch up and eventually, nickel active sites start deactivating due to their coverage with deposited carbon, leading to rapid catalyst deactivation (Zhang et al. 2011). In the case of feed gas flow rates or space velocities, it is evident that higher space velocities cause quick deactivation of catalysts in comparison with lower space velocities associated with the competitive imbalance between carbon nucleation and carbon diffusion at higher space velocities. Therefore, higher amounts of hydrogen and carbon are produced at lower space velocities. It can be concluded from the above discussion that both higher space velocities and operating temperatures lead to catalyst deactivation; however, higher reaction temperature produces more amounts of hydrogen than that of higher space velocities.

In contrast with metal-based catalysts, the deactivation of a carbon-based catalyst is, in fact, a catalyst transformation phenomenon in which active sites in the fresh catalyst sample change to inactive/deactivated sites in the post-reaction catalyst sample. It can be inferred that in carbon-based catalysts, disordered/unstructured types of carbon convert into more structured/ordered carbon. It has been reported that the activation energy of 227.1 kJ/mol in the case of growth of carbon crystallites is much lower than the activation energy (316.8 kJ/mol) of the formation of carbon nuclei during catalytic decomposition of methane (Muradov et al. 2005). The activation energy data indicate that crystallite growth outperforms nucleation rate, and this rapid crystallite growth of carbon could result in turbostratic and/or pseudo-order carbon formation, leading to activity loss. The operating conditions are found to play a role in influencing the catalyst's capacity in accommodating the carbon, hence implying that the amount of carbon formed is not the sole factor behind catalyst deactivation (Moliner et al. 2005). The impact of operating conditions can be divided into two categories: activated diffusion effect (ADE) and molecular sieve effect (MSE). In the case of the activated diffusion effect, methane diffuses in the molecular form inside the smaller-sized pores, and this molecular methane diffusion rate increases at elevated reaction temperatures, leading to enhanced carbon deposition inside pores. Hence, catalytic methane decomposition over-activated carbon catalysts take place inside pores at elevated temperatures. In the molecular sieve effect, carbon deposition is strongly related to blockage of the pore mouth. In fact, with the progression of carbon formation, the pore mouth starts to shrink, leading to loss of access to the inner surface of the pores for methane adsorption/activation. It can be concluded that in the case of carbon-based catalysts, loss of active sites is not only controlled by carbon formation, but experimental parameters also affect the rate of catalyst deactivation as demonstrated by the activated diffusion effect and molecular sieve effect (Ashik et al. 2015).

In conclusion, catalyst deactivation during catalytic methane decomposition is primarily attributed to high-temperature metal sintering and co-product carbon formation. The diverse catalyst behaviors observed underscore the complexity of this process. Sintering, characterized by metal particle enlargement and support structural changes, is irreversible and influences catalyst stability. Carbon formation, on the other hand, occurs due to methane decomposition over active sites and subsequent carbon growth, ultimately encapsulating the catalyst's active sites and leading to deactivation. Operating conditions such as temperature and gas flow rates

Table 5 Effect of different catalysts, gas hourly space velocity, and temperature on carbon yield and types in the catalytic decomposition of methane

Catalysts	Support	Temperature (°C)	GHSV (mL/g_{cat}.h)	Gram (carbon)/gram (CH_{4feed})	Gram (carbon)/gram (catalyst)	Carbon morphology	References
50 wt% Ni	SiO_2	750	1800	0.504	Not available	Carbon nanotubes	Saraswat and Pant (2013b)
50 wt% Ni/5 wt% Cu				0.531	Not available		
50 wt% Ni/10 wt% Cu				0.619	Not available		
50 wt% Ni/15 wt% Cu				0.467	Not available		
50 wt% Ni/20 wt% Cu				0.374	Not available		
50 wt% Ni	MCM-22	750	1800	Not available	3.63	Multi-walled carbon nanotubes	Saraswat and Pant (2011)
50 wt% Ni/5 wt% Cu				Not available	4.26		
50 wt% Ni/5 wt% Cu/5 wt% Zn				Not available	4.26		
50 wt% Ni/10 wt% Cu				Not available	5.5		
50 wt% Ni/10 wt% Zn				Not available	5.45		
$Ni_{0.5}$/Al	Mixed metal oxides (MMOs)	700	6000	Not available	0.11	Carbon nanotubes	Guo et al. (2018)
Ni_1/Al				Not available	0.49		
Ni_2/Al				Not available	2.02		
Ni_3/All				Not available	4.55		
$Ni_{0.5}$	Al_2O_3			Not available	0.67		
Ni_1				Not available	1.15		
Ni_2				Not available	1.36		
Ni_3				Not available	1.29		
85%Fe	ZrO_2	700	8000	Not available	13.5	Carbon nanotubes	Ermakova and Ermakov (2002)
	Al_2O_3			Not available	14		
	TiO_2			Not available	17.4		
	SiO_2			Not available	45		
69 wt% Fe	Al_2O_3	700	6000	Not available	2.28	Multi-walled carbon nanotubes	Torres et al. (2012)
		800	6000	Not available	4.25		
		850	6000	Not available	2.30		
		900	6000	Not available	3.02		
		800	3000	Not available	3.6		
		800	8000	Not available	4.8		
12.3Fe/1Mo (molar ratio)	Al_2O_3	750	1500	Not available	1.92	Bamboo shaped	Torres et al. (2014)
	MgO	750	1500	Not available	8.26	Tubular	
Carbopack C	No support	850	3800	Not available	0.08	Carbon crystallites	Suelves et al. (2007)
Carbopack B			3800	Not available	0.12		
Carbon black (Fluke 05120)			3800	Not available	0.65		
Carbon black (Fluke 05120)			9500	Not available	0.69		

Table 5 (continued)

Catalysts	Support	Temperature (°C)	GHSV (mL/g_{cat}.h)	Gram (carbon)/gram (CH_{4feed})	Gram (carbon)/gram (catalyst)	Carbon morphology	References
Carbon black (Fluke 03866)			3800	Not available	0.212		
Carbon black (Black pearls 2000)			3800	Not available	0.22		
Industrial carbon black (HS-50)			3800	Not available	0.28		
Commercial activated carbon (CG Norit)			3800	Not available	0.45		
Commercial activated carbon (CG Norit)			9500	Not available	0.60		

This comprehensive table showcases the crucial role played by catalyst composition, support material, and operating conditions in determining both the carbon yield and morphology during the catalytic decomposition of methane. By systematically varying these parameters, valuable insights have been gained, enabling the optimization of the process for the production of desired carbon products with enhanced efficiency and selectivity. The findings presented here offer significant contributions toward the development of optimized catalytic systems, particularly for the synthesis of specific carbon products such as carbon nanotubes and multi-walled carbon nanotubes, which hold great potential for diverse applications across various industries. GHSV refers to gas hourly space velocity, and CH_{4feed} refers to methane feed

play crucial roles in catalyst performance, affecting carbon deposition and pore blockage. Understanding these mechanisms is pivotal for designing robust catalysts for methane decomposition applications.

Catalyst regeneration

The regeneration of the deactivated catalyst is the key issue for a continuous hydrogen production method. The researchers frequently propose two different catalyst regeneration techniques: air regeneration Eq. (1) and steam regeneration Eq. (2), with carbon dioxide regeneration Eq. (3) being utilized to a lesser extent. Air regeneration involves oxygen reacting with deposited carbon, resulting in a mixture of carbon oxides. Carbon dioxide regeneration involves carbon reacting with carbon dioxide, producing carbon monoxide and a mixture of carbon oxides. The best method depends on the operation's overall economics. The conclusion remarks of the regeneration test for different catalysts are summarized in Table 6**.**

$$C + O_2 \rightarrow CO_2 \quad \Delta H_{1073} = -394.7 \text{ kJ/mol} \tag{1}$$

$$C + H_2O \rightarrow CO + H_2 \quad \Delta H_{1073} = 135.9 \text{ kJ/mol} \tag{2}$$

$$C + CO_2 \rightarrow CO \quad \Delta H_{1073} = 174.5 \text{ kJ/mol} \tag{3}$$

The steam regeneration of used catalysts is divided into two stages: pure hydrogen production in the first stage and hydrogen polluted with carbon monoxide and carbon dioxide in the second (Zhang and Amiridis 1998). They regenerated a deactivated 16.4% Ni/SiO_2 at 550 °C under a steam environment, restoring its activity and revealing nickel's metallic form and carbon pockets. Transmission electron microscopy results showed filamentous residual carbon with thinner walls, suggesting that initial solid filaments were more resistant to steam gasification. Therefore, it is suggested to propose an air oxidation cycle followed by consecutive cycles to eliminate resistant carbon.

From an energy perspective, utilizing a technology capable of generating sufficient energy to offset a portion of the energy required for methane cracking is highly desirable. One such technology is air regeneration, which offers distinct advantages. In contrast, steam regeneration results in increased hydrogen production; however, it is an endothermic process. On the other hand, air regeneration is exothermic, providing an additional energy benefit. Moreover, the faster the regeneration process, the higher the catalyst circulation rates can be achieved. Notably, air regeneration outperforms steam regeneration in terms of speed. It is worth mentioning that during air regeneration, localized hotspots may arise, leading to the oxidation of specific active sites. Consequently, a reduction step is necessary before reusing the catalyst for methane cracking (Zhang and Amiridis 1998). Sintering can occur in high-temperature zones, reducing the exposed nickel surface area (Aiello et al. 2000). In steam regeneration, on the other hand, the catalyst bed temperature may be kept more homogenous, preventing sintering. Steam regeneration prevents sintering by maintaining a homogeneous catalyst bed temperature. Additionally, the reduction of catalytic activity

after regeneration is due to a shift in nickel atom orientation from nickel (Rahman et al. 2006).

Economics

Currently, hydrogen production is still dominated produced from fossil energy sources such as coal, natural gas, and oil, of which 76% comes from natural gas, 23% from coal, and less than 2% arises from water electrolysis (Zhang et al. 2022). Color codes are frequently used in manufacturing processes to differentiate between different kinds of hydrogen generation and power use, as shown in Fig. 9. Methane reforming methods are commonly utilized for hydrogen generation and emit massive volumes of carbon dioxide, which not only pollute the environment but also need the deployment of downstream treatments owing to the growth in carbon dioxide emission tariffs. Hydrogen from steam methane reforming has an emission factor of around 285 g/kWh-H_2 (9.5 $kgCO_2/kgH_2$), and coal gasification has an emission factor of around 675 g/kWh-H_2, accounting only for energy use and process emissions (IRENA 2019). Additional carbon dioxide separation steps (Wibowo et al. 2021), carbon capture and storage (CCS) (Zhang et al. 2022), and carbon capture and utilization (CCUS) (Lim et al. 2023) need to be considered.

On the other hand, methane decomposition has the lowest specific economic emissions of 40 $kgCO_2/MWh_{H2}$ compared to steam methane reforming (293 $kgCO_2/MWh_{H2}$) and even steam methane reforming coupled with carbon capture and storage (133 $kgCO_2/MWh_{H2}$). In the case of electrolysis, the specific carbon dioxide emissions are influenced by electricity production technologies; besides using renewable electricity for electrolysis, higher specific carbon dioxide emissions cannot be avoided. At present, carbon capture and storage technologies are performed by capturing carbon dioxide in the gaseous form and transporting it to the storage site. However, carbon capture and storage needs considerable investment in infrastructure, and thus, its implementation is still a time-consuming process and may increase the price of hydrogen.

The techno-economic evaluations of several hydrogen production technologies are recently reported. Parkinson et al. (2019) estimated that the costs of current hydrogen production from steam methane reforming range from 1.52 to 2.32 USD/kgH_2, with an average of 1.89 USD/kgH_2 for natural gas prices from 4.80 to 12.26 USD/GJ. The production of hydrogen by steam methane reforming, coal and biomass gasification, and water electrolysis has been economically studied (Mueller-Langer et al. 2007). Their study revealed that steam methane reforming is currently the most favorable hydrogen production method from a techno-economic point of view. The specific total capital investment and hydrogen production cost of steam methane reforming without carbon capture and storage were calculated to be 522,475 USD/MW_{th} and 60 USD/MW_{th}, respectively. Higher specific total capital investment and hydrogen production cost were found for steam methane reforming with carbon capture and storage, which is approximately 598,773 USD/MW_{th} and 66 USD/MW_{th}, respectively. Likewise, Simbeck and Chang found steam methane reforming to be a less expensive hydrogen generation technique than coal gasification, biomass gasification, petroleum coke gasification, and/or water electrolysis (Simbeck 2002). They found that the production of hydrogen from steam methane reforming varied and was affected by the sequential hydrogen delivery. Additionally, the production cost of large-scale steam methane reforming also depends on the natural cost price (share of 70–75%) and an extra 10–23% of the cost for carbon capture and storage (Mueller-Langer et al. 2007).

Gasification of coal could be competitive with steam methane reforming when the price of natural gas is enormously high. The hydrogen production cost available in the literature is 1.42–2.77 USD/kgH_2 (average of 2.04 USD/kgH_2) for coal prizes from 1.96 to 4.03 USD/GJ (Parkinson et al. 2019). Compared to steam methane reforming, the specific total capital investment of coal gasification without and with carbon capture and storage were 1,273,844 USD/MW_{th} and 1,459,612 EURO/$MW_{th,}$ respectively (Mueller-Langer et al. 2007). Mueller-Langer et al. (2007) calculated that the production cost of hydrogen from coal gasification with carbon capture and storage is around 65 EURO/MW_{th}, which is more expensive than that of without carbon capture and storage (50 EURO/MW_{th}). The lower hydrogen production cost might be explained by the lower coal price compared with the natural gas price. Currently, there are only a few commercial uses of biomass gasification for hydrogen generation; however, if the present technological limitations are overcome, this can be a financially feasible choice. The supply chain and price of various biomass feedstocks have a significant impact on the sustainable operation of biomass gasification plants. It is believed that the utilization of biomass will receive more and more attention to deal with net zero emissions.

On the other hand, hydrogen production by electrolysis of water has recently been developed as it can be powered by renewable electricity. Yet, electrolysis cannot be applied in wide-scale hydrogen production to meet the hydrogen economy due to the cost of electrolyzers and renewable electricity. The lower production costs of renewable electricity could be achieved when the capital investment for renewable electricity production plants can be reduced. The specific investment of water electrolysis and the production cost of hydrogen are estimated to reach 1.82 million USD/MW_{th} and 130 USD/MW_{th}, respectively

Table 6 Catalyst regeneration under different operating conditions and oxidative agents

Catalyst	Oxidative agent	Regeneration temperature (°C)	Concluding remarks	References
$40Fe/Al_2O_3$	Carbon dioxide	750	The regeneration catalyst would not be able to agglomerate as big as the fresh catalyst and could not completely oxidize deposited carbon by carbon dioxide oxidation due to the limited oxidation capacity of carbon dioxide	Qian et al. (2019)
Fe/SiO_2	10% oxygen	500	Carbon deposition was burnt off as carbon dioxide. The regeneration could maintain the catalyst activity, but the selectivity toward carbon nanotubes formation decreased	Ayillath Kutteri et al. (2018)
$Ni/CeZrO_2$	2.8 vol% H_2O/Argon	900	The oxidation of deposited carbon took place at lower temperatures, and the complete regeneration was obtained at 650 °C. The formation of hydrogen was not only from the carbon oxidation but also water dissociation on zero-valent nickel and oxygen vacancy of $CeZrO_2$	Lamacz (2019)
Activated carbon	Carbon dioxide	900–1000	Higher regeneration temperature increased the long-term stability of the catalyst	Abbas and Daud (2009)
Ni/MgO	2.8 vol% H_2O/Argon	900	The carbon on the Ni/MgO was oxidized at 700 °C, but re-oxidation was not complete. Hydrogen was produced from the oxidation of carbon deposits and partial re-oxidation of the nickel	Lamacz (2019)
CG-Norit	Carbon dioxide	925	High temperatures are required to effectively remove all remaining carbon that has impacted the textural properties of the catalyst	Pinilla et al. (2007)
$Ni/?\text{-}Al_2O_3$	Air	500	After oxygen regeneration, the catalyst fragmented into a fine powder, presumably due to regeneration or porous alumina support disintegration during filament growth	Rahman et al. (2006)
$15Co\text{-}30Fe/Al_2O_3$	10% oxygen/nitrogen	500	The performance of regenerated catalysts showed a lower activity at a higher cycle number. The coke deposition could be the reason for deactivating the catalyst. Thus, some of the iron active sites of catalyst could not completely regenerated	Fakeeha et al. (2018c)

The table presents a comprehensive overview of catalyst regeneration procedures, considering various operating conditions and oxidative agents. Each regeneration method, including air, steam, and carbon dioxide, exerts distinct effects on catalyst performance and longevity. Steam regeneration stands out for its ability to enhance hydrogen production while maintaining catalyst stability. On the other hand, carbon dioxide regeneration exhibits notable impacts on catalytic activity over repeated cycles. Crucial information regarding temperature effects and observed changes in catalyst behavior is provided for each entry. This comprehensive understanding of different regeneration pathways is vital for optimizing catalyst performance in continuous hydrogen production processes

(Mueller-Langer et al. 2007). Regardless of this, water electrolysis may likely be practical for regions without access to natural gas (remote areas or standalone grids), or if hydrogen is applied as an energy storage of electricity. The techno-economic evaluation of hydrogen production by dual fluidized bed biomass gasification (DFB), biogas steam reforming (BSR), and electrolysis with their necessary downstream separation and purification steps was reported (Yao et al. 2017).

Many academics have suggested the catalytic decomposition of methane to produce hydrogen as a viable transition technology toward the hydrogen economy. The production cost of hydrogen from the catalytic decomposition of methane is expected to be 1.57–1.67 USD/kgH_2 (Yousefi Rizi and Shin 2022). When the value of the carbon product (carbon black) exceeds 611 USD/ton-carbon, and the cost of carbon dioxide emission allowance is less than 49 USD/tonCO_2, hydrogen generation based on catalytic decomposition of methane would be economically feasible (Yuan et al. 2008). Meanwhile, it was reported that the thermal decomposition of methane (TDM) would be competitive with steam reforming when the product carbon value of 295 USD/ton-carbon and carbon tax of 115 USD/ton-CO_2 are achieved (Parkinson et al. 2019). Carbon black is composed of elemental carbon with tiny particle sizes and may be utilized as a reinforcing ingredient in rubber goods as

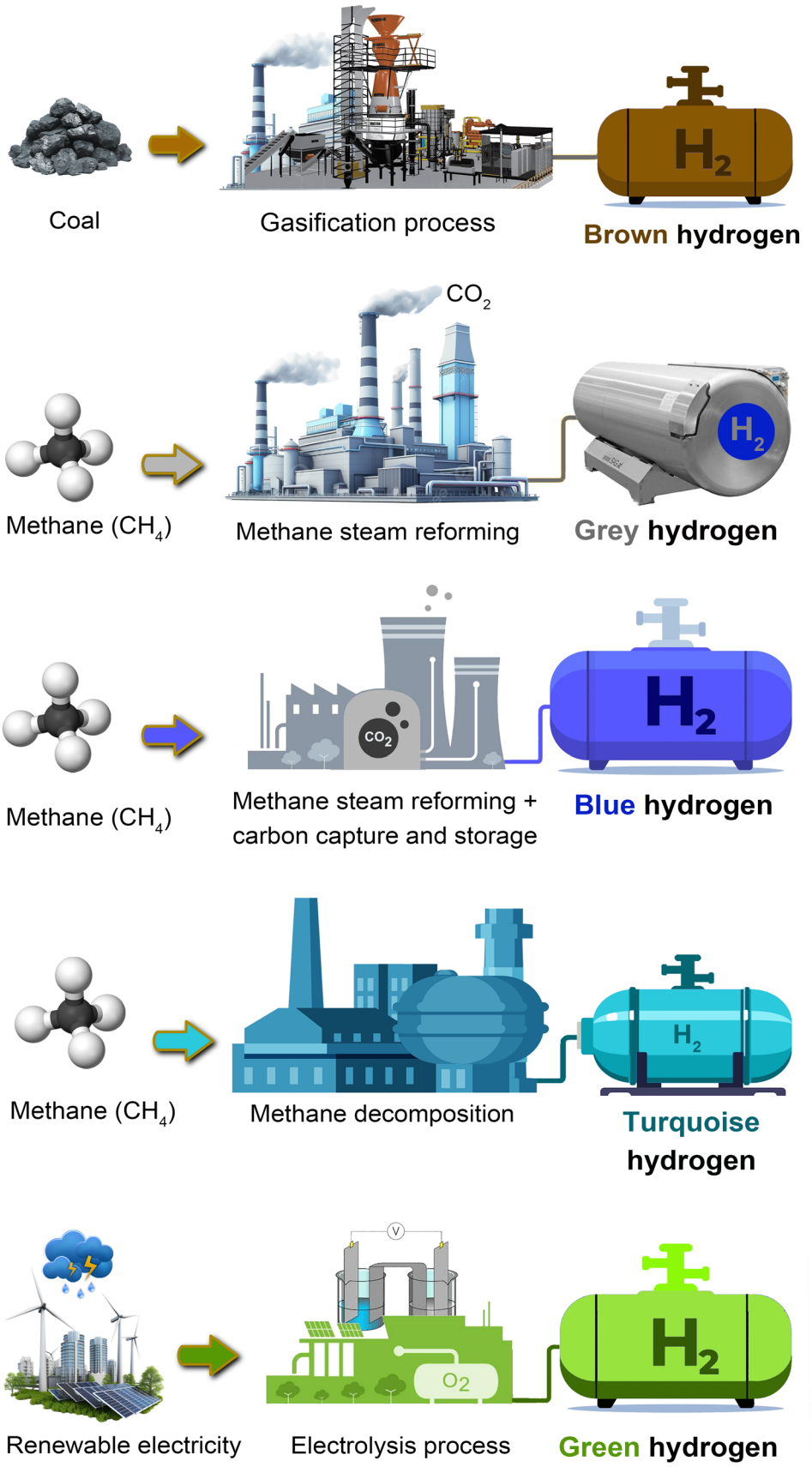

Fig. 9 Hydrogen production pathways. The manufacturing processes employ hydrogen color coding, distinguishing between different hydrogen types based on their production methods. Green hydrogen, generated from renewable energy sources such as solar or wind energy, undergoes water electrolysis. Gray and brown hydrogen result from methane steam reforming and coal gasification, respectively. Blue hydrogen is produced by combining either gray or brown hydrogen with carbon capture and storage techniques. Turquoise hydrogen, derived from methane pyrolysis, yields solid carbon as a by-product

well as a pigment source in paints and inks. Carbon black costs between 500 and 2000 EURO per ton, depending on quality (Keipi et al. 2018). It has also been reported that the catalytic decomposition of methane could produce various carbon, which has economic value (Mitoura dos Santos Junior et al. 2022).

The estimated prices of carbon products produced from methane decomposition, as found in a study by Mitoura dos Santos Junior et al. (2022), are as follows: Carbon black ranges from 400 to 2000 USD per ton, carbon fibers range from 25,000 to 113,000 USD per ton, and carbon nanotubes have an estimated price range of 100,000–600,000 USD per ton.

Keipi et al. (2018) conducted a comprehensive cost–benefit analysis of hydrogen generation methods including methane decomposition, steam reforming, and water electrolysis on a small, medium, and large scale. The results showed that the product of carbon plays an economical role in small or medium industrial-scale on-site hydrogen production. The cost of centralized hydrogen production by steam reforming methane is very cheap; however, the necessity for hydrogen transportation raises the cost of hydrogen production. The cost of hydrogen transportation has been calculated to be 75 USD/MWh_{H2} for transportation distances longer than 100 km and 36 USD/ MWh_{H2} for distances less than 50 km (Yang and Ogden 2007).

In conclusion, as methane decomposition does not produce carbon dioxide, it will be more competitive than other technologies for hydrogen production for industrial applications. Strict regulation is needed to deal with this issue. Furthermore, for a thorough economic and environmental evaluation of hydrogen energy chains, the additional expenses for hydrogen storage, transportation, and consumption should be addressed. Despite their economic competitiveness, large-scale hydrogen plants have hurdles because of the increased effort required to create the infrastructure network for storage, transmission, and distribution. A small–moderate-size hydrogen production facility, on the other hand, would allow for the alleviation of these concerns at the penalty of increased hydrogen production costs. Therefore, a comprehensive assessment of hydrogen production, storage, distribution, and utilization needs to be economically analyzed, depending on the needs of specific regions. A summary of hydrogen production is listed in Table 7 to give insight into hydrogen production from different pathways.

Perspective

Catalytic methane decomposition has been investigated for over a century; however, this technology has yet to be commercialized and faces severe challenges. The catalyst is currently being designed in the laboratory, and the most significant challenge is catalytic activity loss caused by poisoning, coking (carbon deposition), mechanical deterioration, and sintering. It is difficult for catalysts to exhibit both high activity and long-term stability. The fundamental issue is that carbon, an unavoidable by-product of catalytic methane decomposition, hinders active sites from interacting with methane. A considerable deal of study has been done on the deactivation process. Deactivation through carbon encapsulation is the primary mechanism of catalyst inactivation. Higher methane conversion rates are achieved by some metal-based catalysts at the expense of increasing carbon dioxide emissions. The oxygen molecules are acquired mostly from the support or from oxygen-containing functional groups on the support surfaces, reducing the benefits of catalytic methane decomposition. Furthermore, metal carbide production causes deactivation, which is a significant barrier to employing metal-based catalysts.

The specific impact of carbon surface structure on catalytic methane decomposition performance in carbon-based catalysts is currently under discussion. Although faults and outlying edges are commonly mentioned as being important in the formation of active cores, there is no direct crucial proof. Controlling these areas intentionally and successfully throughout the preparatory phase remains challenging. Controlling the initial carbon catalyst and the produced carbon during the catalytic methane decomposition reaction, which might result in an autocatalytic reaction process, is complex. Although the synergistic effect of metal and carbon is often utilized to explain catalyst activity augmentation, the particular approach and procedure are unknown.

Many studies indicate that regeneration of the catalyst is the best technique for overcoming deactivation. Even ignoring the issue of retaining the activity of the regenerated catalyst, catalyst regeneration encounters secondary emissions and carbonaceous waste. According to studies, the amount of carbon dioxide and/or carbon monoxide generated during the regeneration process is roughly similar to that produced during the steam reforming process. This not only decreases efforts to regulate emissions, but it may also contaminate the generated hydrogen, needing further purification to get clean hydrogen.

As a result, the regeneration process has had a significant impact on the primary aim of the catalytic methane decomposition development. Carbon is widely regarded as a high-value-added commodity that necessitates the separation of carbon and catalyst. The unique characteristics of carbon allow for a wide range of applications (Fig. 10). Another key issue is knowing how to appropriately collect carbon without interfering with the function of the catalyst. Finally, finding a market for the carbon produced in the process is a crucial hurdle before considering commercial implementation. According to the catalytic methane decomposition process's economic analysis, the sales price of carbon products

Table 7 Recent hydrogen production costs via different routes

Process conversion	Capital cost (million USD)	Plant size (ton/day)	Feedstock price (USD/GJ)	Hydrogen cost		References
				USD/kg	USD/GJ	
Steam reforming	591	1200	7.70	1.96	11.72	Council (2004)
	33	379	9.86	3.00	21.11	Ramsden et al. (2013)
	148	120.5	4.87	1.65	11.63	Molburg and Doctor (2003)
	268	298.8	12.26	2.70	19.05	Mueller-Langer et al. (2007)
	591	1200	7.70	1.96	11.72	Council (2004)
	107	150	6.70	1.68	11.81	Ewan and Allen (2005)
	356	446	3.91	1.58	11.13	Khojasteh Salkuyeh et al. (2017)
	Not available	87	Not available	Not available	Not available	Muradov (2000)
	245	208.8	6.60	3.19	22.42	Keipi et al. (2018)
Steam reforming with carbon capture and storage	Not available	Not available	Not available	1.83	12.93	Council (2004)
	Not available	Not available	Not available	2.23	15.69	Molburg and Doctor (2003)
	Not available	Not available	Not available	2.98	20.94	Mueller-Langer et al. (2007)
	Not available	Not available	Not available	2.69	18.94	Ewan and Allen (2005)
	Not available	Not available	Not available	1.80	12.68	Hosseini and Wahid (2016)
	Not available	Not available	Not available	3.19	22.45	(Khojasteh Salkuyeh et al. 2017)
	Not available	Not available	Not available	2.52	17.77	Muradov (2000)
	Not available	Not available	Not available	4.15	29.18	Keipi et al. (2018)
Coal gasification	1609	1200	2.10	1.28	9.00	Council (2004)
	1732	770.7	2.55	1.74	12.24	Kreutz et al. (2005)
	652	298.8	4.03	2.24	15.85	Mueller-Langer et al. (2007)
	423	150	2.11	2.29	16.12	Ewan and Allen (2005)
Coal gasification with carbon capture and storage	Not available	Not available	Not available	1.95	13.70	Council (2004)
	Not available	Not available	Not available	3.32	23.44	Davison et al. (2009)
	Not available	Not available	Not available	2.33	16.41	Mueller-Langer et al. (2007)
	Not available	Not available	Not available	3.13	22.08	Ramsden et al. (2013)
Methane decomposition	422	196.5	1.03	2.89	20.44	Mondal and Ramesh Chandran (2014)
	8	2.16	10.15	3.62	25.42	Keipi et al. (2018)
	849	547	5.90	2.39	16.85	Parkinson et al. (2017)
	515	274	5.90	2.05	14.45	Parkinson et al. (2018) Parkinson et al. (2017)
	242	152.9	7.54	2.15	15.22	Lane and Spath (2018)
Water electrolysis						
Wind electrolysis	1033 USD/kW	Not available	Not available	6.14–7.44	43.24–52.39	Levene and Sverdrup (2006)
	738 USD/kW	Not available	Not available	10.30	72.51	Nikolaidis and Poullikkas (2017)
	1328 USD/kW	Not available	Not available	5.25	36.97	Mason (2007)

Table 7 (continued)

Process conversion	Capital cost (million USD)	Plant size (ton/day)	Feedstock price (USD/GJ)	Hydrogen cost		References
				USD/kg	USD/GJ	
Solar electrolysis	590 USD/kW	Not available	Not available	8.80–35.41	61.93–249.28	Nikolaidis and Poullikkas (2017)
	1353 USD/kW	Not available	Not available	4.93	34.68	Mason (2007)
Nuclear electrolysis	1181 USD/kW	Not available	Not available	9.15–10.52	64.5–74.11	Parkinson et al. (2017)
	738 USD/kW	Not available	Not available	6.13–11.78	46.77–82.95	Nikolaidis and Poullikkas (2017)

It highlights capital costs, plant sizes, feedstock prices, and resulting hydrogen costs across different processes such as steam reforming, coal gasification, methane decomposition, and water electrolysis (including wind, solar, and nuclear electrolysis). The data underscore the economic viability and comparative advantages of each production route. While steam reforming remains prevalent despite high capital expenses, methane decomposition emerges as a potentially cost-effective alternative. Water electrolysis, particularly utilizing renewable energy sources, offers environmentally sustainable options with competitive hydrogen costs. Nuclear electrolysis presents a promising avenue with relatively lower capital outlays. This comprehensive analysis aids policymakers, researchers, and industry stakeholders in navigating the evolving landscape of hydrogen production economics, facilitating informed decisions on technology adoption and investment

and methane are the most important factors impacting the economic feasibility of hydrogen generation.

Conclusion

This review paper provides a comprehensive analysis of catalytic methane decomposition for carbon–neutral hydrogen production. The escalating global demand for energy, coupled with the need to reduce greenhouse gas emissions, highlights the significance of exploring sustainable energy carriers such as hydrogen. The review emphasizes the potential of catalytic methane decomposition as a promising avenue for hydrogen production, along with the synthesis of valuable carbon nanomaterials. The review highlights the advancements in catalyst development for catalytic methane decomposition, including metal-based catalysts such as monometallic, bimetallic, and trimetallic catalysts. It also explores the role of carbon-based catalysts and the significance of support materials in enhancing catalytic performance. The analysis of catalyst deactivation mechanisms, particularly coke deposition and metal sintering, sheds light on the challenges associated with catalytic methane decomposition. However, the review underscores the importance of catalyst regeneration techniques to maintain catalyst activity and prolong its lifespan.

From an economic perspective, the review evaluates the feasibility of catalytic methane decomposition and its potential for cost-effective hydrogen production. With global hydrogen demand projected to increase significantly in the coming years, catalytic methane decomposition offers a promising solution due to its lower energy requirements and simplified process compared to traditional reforming methods. The review also emphasizes the need for further research and development to address the challenges and optimize the economic viability of catalytic methane decomposition. Statistical data from the review support the significance of catalytic methane decomposition as a sustainable energy production method. The projected increase in global hydrogen demand from 70 million tons in 2019 to over 200 million tons in 2030 underscores the growing importance of hydrogen as an energy carrier. The analysis of different hydrogen production processes, including steam reforming, dry reforming, and partial oxidation of methane, highlights the advantages and limitations of each method. The moderate endothermic nature of catalytic methane decomposition, resulting in lower energy requirements and operational costs, further strengthens its potential as a viable option for hydrogen production. Overall, this review paper provides valuable insights into the catalytic methane decomposition process, catalyst development, deactivation mechanisms, regeneration techniques, and economic considerations. It serves as a roadmap for future research and development in catalytic methane decomposition, aiming to contribute to the sustainable evolution of hydrogen production technologies in the broader context of environmental chemistry. By harnessing the potential of catalytic methane decomposition, we can pave the way for a carbon–neutral future and mitigate the challenges associated with energy supply and greenhouse gas emissions.

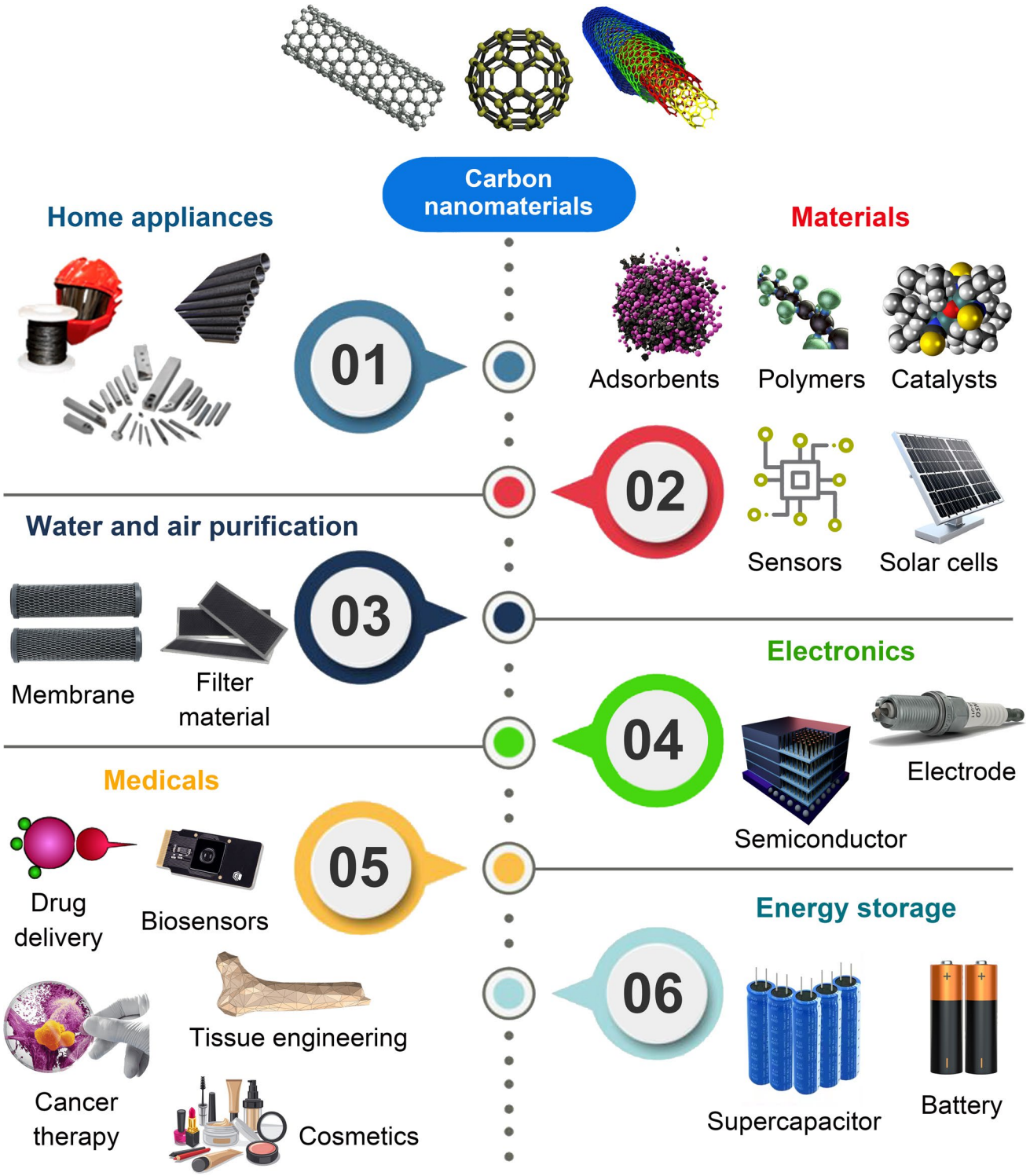

Fig. 10 Applications of carbon nanomaterials. Carbon nanomaterials, including single-walled nanotubes, fullerene, multi-walled nanotubes, graphene, and their composites, are being applied in many fields. Due to their special properties, carbon nanomaterials have been utilized for energy storage, such as batteries and supercapacitors, polymer and composite materials, membranes, nanocatalysts, adsorbents, and sensors. Recently, biomedical fields also use carbon materials for medical purposes such as drug delivery, biomedical imaging and sensors, tissue engineering, and canter therapy

Acknowledgements The author(s) would like to acknowledge the support provided by the Deanship of Research Oversight and Coordination (DROC) at King Fahd University of Petroleum and Minerals (KFUPM) for funding this work through project # KU201002.

Declarations

AIO declares that he is Editor of Environmental Chemistry Letters.

Conflict of interest The authors declare that they have no known competing financial interests or personal relationships that could have appeared to influence the work reported in this paper.

References

Abbas HF, Daud WMAW (2009) Thermocatalytic decomposition of methane for hydrogen production using activated carbon catalyst: regeneration and characterization studies. Int J Hydrog Energy 34:8034–8045. https://doi.org/10.1016/j.ijhydene.2009.08.014

Ahmed W et al (2016) Ni/CeO_2–Al_2O_3 catalysts for methane thermocatalytic decomposition to CO-free H_2 production. Int J Hydrog Energy 41:18484–18493. https://doi.org/10.1016/j.ijhydene.2016.08.177

Aiello R et al (2000) Hydrogen production via the direct cracking of methane over Ni/SiO_2: catalyst deactivation and regeneration. Appl Catal A Gen 192:227–234. https://doi.org/10.1016/S0926-860X(99)00345-2

Al Mesfer MK et al (2021) Synthesis, evaluation, and kinetic assessment of Co-based catalyst for enhanced methane decomposition reaction for hydrogen production. Int J Chem Kinet 54:90–103. https://doi.org/10.1002/kin.21544

Alalga L et al (2021) Hydrogen production via methane decomposition over nickel supported on synthesized ZSM-5/MCM-41 zeolite composite material. Int J Hydrog Energy 46:28501–28512. https://doi.org/10.1016/j.ijhydene.2021.06.090

Al-Fatesh AS et al (2016) Production of hydrogen by catalytic methane decomposition over alumina supported mono-, bi- and trimetallic catalysts. Int J Hydrog Energy 41:22932–22940. https://doi.org/10.1016/j.ijhydene.2016.09.027

Al-Fatesh AS et al (2020) Catalytic methane decomposition over ZrO_2 supported iron catalysts: effect of WO_3 and La_2O_3 addition on catalytic activity and stability. Renew Energy 155:969–978. https://doi.org/10.1016/j.renene.2020.04.038

Al-Fatesh AS et al (2025) Iron-promoted zirconia-alumina supported Ni catalyst for highly efficient and cost-effective hydrogen production via dry reforming of methane. J Environ Sci 148:274–282. https://doi.org/10.1016/j.jes.2023.06.024

Alptekin FM, Celiktas MS (2022) Review on catalytic biomass gasification for hydrogen production as a sustainable energy form and social, technological, economic, environmental, and political analysis of catalysts. ACS Omega 7:24918–24941. https://doi.org/10.1021/acsomega.2c01538

Alves L et al (2021) Catalytic methane decomposition to boost the energy transition: scientific and technological advancements. Renew Sustain Energy Rev 137:110465. https://doi.org/10.1016/j.rser.2020.110465

Amin AM et al (2011) Review of methane catalytic cracking for hydrogen production. Int J Hydrog Energy 36:2904–2935. https://doi.org/10.1016/j.ijhydene.2010.11.035

Ampelli C et al (2014) Carbon-based catalysts: opening new scenario to develop next-generation nano-engineered catalytic materials. Chin J Catal 35:783–791. https://doi.org/10.1016/S1872-2067(14)60139-X

Aramouni NAK et al (2018) Catalyst design for dry reforming of methane: analysis review. Renew Sustain Energy Rev 82:2570–2585. https://doi.org/10.1016/j.rser.2017.09.076

Araújo PM et al (2021) Hydrogen production from methane autothermal reforming over $CaTiO_3$, $BaTiO_3$ and $SrTiO_3$ supported nickel catalysts. Int J Hydrog Energy 46:24107–24116. https://doi.org/10.1016/j.ijhydene.2021.04.202

Argyle MD, Bartholomew CH (2015) Heterogeneous catalyst deactivation and regeneration: a review. Catalysts 5:145–269h

Arku P et al (2018) A review of catalytic partial oxidation of fossil fuels and biofuels: recent advances in catalyst development and kinetic modelling. Chem Eng Res Des 136:385–402. https://doi.org/10.1016/j.cherd.2018.05.044

Ashik UPM et al (2015) Production of greenhouse gas free hydrogen by thermocatalytic decomposition of methane—a review. Renew Sustain Energy Rev 44:221–256. https://doi.org/10.1016/j.rser.2014.12.025

Awad A et al (2019) Non-oxidative decomposition of methane/methanol mixture over mesoporous $Ni–Cu/Al_2O_3$ Co-doped catalysts. Int J Hydrog Energy 44:20889–20899. https://doi.org/10.1016/j.ijhydene.2018.04.233

Awadallah AE, Aboul-Enein AA (2015) Catalytic decomposition of methane to COx-free hydrogen and carbon nanotubes over Co–W/MgO catalysts. Egypt J Pet 24:299–306. https://doi.org/10.1016/j.ejpe.2015.07.008

Awadallah AE et al (2013a) Various nickel doping in commercial $Ni–Mo/Al_2O_3$ as catalysts for natural gas decomposition to COx-free hydrogen production. Renew Energy 57:671–678. https://doi.org/10.1016/j.renene.2013.02.024

Awadallah AE et al (2013b) Direct conversion of natural gas into COx-free hydrogen and MWCNTs over commercial $Ni–Mo/Al_2O_3$ catalyst: effect of reaction parameters. Egypt J Pet 22:27–34. https://doi.org/10.1016/j.ejpe.2012.11.012

Awadallah AE et al (2013c) Novel aluminosilicate hollow sphere as a catalyst support for methane decomposition to COx-free hydrogen production. Appl Surf Sci 287:415–422. https://doi.org/10.1016/j.apsusc.2013.09.173

Awadallah AE et al (2014a) Catalytic thermal decomposition of methane to COx-free hydrogen and carbon nanotubes over MgO supported bimetallic group VIII catalysts. Appl Surf Sci 296:100–107. https://doi.org/10.1016/j.apsusc.2014.01.055

Awadallah AE et al (2014b) Hydrogen production via methane decomposition over Al_2O_3–TiO_2 binary oxides supported Ni catalysts: effect of Ti content on the catalytic efficiency. Fuel 129:68–77. https://doi.org/10.1016/j.fuel.2014.03.047

Awadallah AE et al (2016a) Effect of structural promoters on the catalytic performance of cobalt-based catalysts during natural gas decomposition to hydrogen and carbon nanotubes. Fuller Nanotubes Carbon Nanostruct 24:181–189. https://doi.org/10.1080/1536383X.2015.1132206

Awadallah AE et al (2016b) Effect of crystalline structure and pore geometry of silica based supported materials on the catalytic

behavior of metallic nickel particles during methane decomposition to CO-free hydrogen and carbon nanomaterials. Int J Hydrog Energy 41:16890–16902. https://doi.org/10.1016/j.ijhydene.2016.07.081

Awadallah AE et al (2017a) Influence of Mo or Cu doping in Fe/MgO catalyst for synthesis of single-walled carbon nanotubes by catalytic chemical vapor deposition of methane. Fuller Nanotubes Carbon Nanostruct 25:256–264. https://doi.org/10.1080/1536383X.2017.1283619

Awadallah AE et al (2017b) Facile and large-scale synthesis of high quality few-layered graphene nano-platelets via methane decomposition over unsupported iron family catalysts. Mater Chem Phys 191:75–85. https://doi.org/10.1016/j.matchemphys.2017.01.007

Awadallah AE et al (2018) Methane decomposition into COx-free hydrogen and carbon nanomaterials over ZrO_2–M (M = MgO, Al_2O_3, SiO_2, La_2O_3 or CeO_2) binary oxides supported cobalt catalysts. Fuller Nanotubes Carbon Nanostruct 27:128–136. https://doi.org/10.1080/1536383x.2018.1523147

Ayillath Kutteri D et al (2018) Methane decomposition to tip and base grown carbon nanotubes and COx-free H_2 over mono- and bimetallic 3d transition metal catalysts. Catal Sci Technol 8:858–869. https://doi.org/10.1039/C7CY01927K

Bai Z et al (2007) Methane decomposition over Ni loaded activated carbon for hydrogen production and the formation of filamentous carbon. Int J Hydrog Energy 32:32–37. https://doi.org/10.1016/j.ijhydene.2006.06.030

Baker RTK et al (1972) Nucleation and growth of carbon deposits from the nickel catalyzed decomposition of acetylene. J Catal 26:51–62. https://doi.org/10.1016/0021-9517(72)90032-2

Bayat N et al (2015) COx-free hydrogen and carbon nanofibers production by methane decomposition over nickel–alumina catalysts. Korean J Chem Eng 33:490–499. https://doi.org/10.1007/s11814-015-0183-y

Bayat N et al (2016a) Hydrogen and carbon nanofibers synthesis by methane decomposition over Ni–Pd/Al_2O_3 catalyst. Int J Hydrog Energy 41:5494–5503. https://doi.org/10.1016/j.ijhydene.2016.01.134

Bayat N et al (2016b) Methane decomposition over Ni–Fe/Al_2O_3 catalysts for production of COx-free hydrogen and carbon nanofiber. Int J Hydrog Energy 41:1574–1584. https://doi.org/10.1016/j.ijhydene.2015.10.053

Bayat N et al (2016c) Thermocatalytic decomposition of methane to COx-free hydrogen and carbon over Ni–Fe–Cu/Al_2O_3 catalysts. Int J Hydrog Energy 41:13039–13049. https://doi.org/10.1016/j.ijhydene.2016.05.230

Carapellucci R, Giordano L (2020) Steam, dry and autothermal methane reforming for hydrogen production: a thermodynamic equilibrium analysis. J Power Sources. https://doi.org/10.1016/j.jpowsour.2020.228391

Cazaña F et al (2018) Synthesis of graphenic nanomaterials by decomposition of methane on a Ni–Cu/biomorphic carbon catalyst. Kinetic and characterization results. Catal Today 299:67–79. https://doi.org/10.1016/j.cattod.2017.03.056

Chesnokov VV, Chichkan AS (2009) Production of hydrogen by methane catalytic decomposition over Ni–Cu–Fe/Al_2O_3 catalyst. Int J Hydrog Energy 34:2979–2985. https://doi.org/10.1016/j.ijhydene.2009.01.074

Council NR (2004) The hydrogen economy: opportunities, costs, barriers, and R&D needs. National Academis Press, Washington

Dasireddy VDBC, Likozar B (2017) Activation and decomposition of methane over cobalt-, copper-, and iron-based heterogeneous catalysts for COx-free hydrogen and multiwalled carbon nanotube production. Energy Technol 5:1344–1355. https://doi.org/10.1002/ente.201600633

Davison J et al (2009) Co-production of hydrogen and electricity with CO_2 capture. Energy Procedia 1:4063–4070. https://doi.org/10.1016/j.egypro.2009.02.213

Deka TJ et al (2022) Methanol fuel production, utilization, and techno-economy: a review. Environ Chem Lett 20:3525–3554. https://doi.org/10.1007/s10311-022-01485-y

Dufour A et al (2008) Catalytic decomposition of methane over a wood char concurrently activated by a pyrolysis gas. Appl Catal A Gen 346:164–173. https://doi.org/10.1016/j.apcata.2008.05.023

Eggenhuisen TM et al (2013) Freeze-drying for controlled nanoparticle distribution in Co/SiO_2 Fischer–Tropsch catalysts. J Catal 297:306–313. https://doi.org/10.1016/j.jcat.2012.10.024

Ermakova MA, Ermakov DY (2002) Ni/SiO_2 and Fe/SiO_2 catalysts for production of hydrogen and filamentous carbon via methane decomposition. Catal Today 77:225–235. https://doi.org/10.1016/S0920-5861(02)00248-1

Ermakova MA et al (2000) Effective catalysts for direct cracking of methane to produce hydrogen and filamentous carbon: Part I. Nickel catalysts. Catal A Gen 201:61–70. https://doi.org/10.1016/S0926-860X(00)00433-6

Ewan BCR, Allen RWK (2005) A figure of merit assessment of the routes to hydrogen. Int J Hydrog Energy 30:809–819. https://doi.org/10.1016/j.ijhydene.2005.02.003

Fakeeha AH et al (2018a) Hydrogen production via catalytic methane decomposition over alumina supported iron catalyst. Arab J Chem 11:405–414. https://doi.org/10.1016/j.arabjc.2016.06.012

Fakeeha AH et al (2018b) Bi-metallic catalysts of mesoporous Al_2O_3 supported on Fe, Ni and Mn for methane decomposition: effect of activation temperature. Chin J Chem Eng 26:1904–1911. https://doi.org/10.1016/j.cjche.2018.02.032

Fakeeha A et al (2018c) In situ regeneration of alumina-supported cobalt-iron catalysts for hydrogen production by catalytic methane decomposition. Catalysts 8:567. https://doi.org/10.3390/catal8110567

Fakeeha AH et al (2020) Methane decomposition over ZrO(2)-supported Fe and Fe–Ni catalysts-effects of doping La(2)O(3) and WO(3). Front Chem 8:317. https://doi.org/10.3389/fchem.2020.00317

Fan Z et al (2021) Catalytic decomposition of methane to produce hydrogen: a review. J Energy Chem 58:415–430. https://doi.org/10.1016/j.jechem.2020.10.049

Figueiredo JL (1982) Carbon formation and gasification on nickel. In: Figueiredo JL (ed) Progress in catalyst deactivation. Springer, Dordrecht, pp 45–63

Franchi G et al (2020) Hydrogen production via steam reforming: a critical analysis of MR and RMM technologies. Membranes (basel). https://doi.org/10.3390/membranes10010010

Gamal A et al (2021) Catalytic methane decomposition to carbon nanostructures and COx-free hydrogen: a mini-review. Nanomaterials. https://doi.org/10.3390/nano11051226

Gao B et al (2019a) Catalytic methane decomposition over bimetallic transition metals supported on composite aerogel. Energy Fuels 33:9099–9106. https://doi.org/10.1021/acs.energyfuels.9b01723

Gao B et al (2019b) Catalytic performance and reproducibility of Ni/Al_2O_3 and Co/Al_2O_3 mesoporous aerogel catalysts for methane decomposition. Ind Eng Chem Res 58:798–807. https://doi.org/10.1021/acs.iecr.8b04223

Gao B et al (2020a) Correction to "Catalytic performance and reproducibility of Ni/Al_2O_3 and Co/Al_2O_3 mesoporous aerogel catalysts for methane decomposition." Ind Eng Chem Res 59:3629–3631. https://doi.org/10.1021/acs.iecr.9b06957

Gao X et al (2020b) A comprehensive review of anti-coking, anti-poisoning and anti-sintering catalysts for biomass tar reforming reaction. Chem Eng Sci X 7:100065. https://doi.org/10.1016/j.cesx.2020.100065

Guil-Lopez R et al (2011) Comparison of metal and carbon catalysts for hydrogen production by methane decomposition. Appl Catal A Gen 396:40–51. https://doi.org/10.1016/j.apcata.2011.01.036
Guo Z et al (2018) Insight into the role of metal/oxide interaction and Ni availabilities on NiAl mixed metal oxide catalysts for methane decomposition. Appl Catal A Gen 555:1–11. https://doi.org/10.1016/j.apcata.2018.01.031
Harun K et al (2020) Hydrogen production via thermocatalytic decomposition of methane using carbon-based catalysts. RSC Adv 10:40882–40893. https://doi.org/10.1039/D0RA07440C
Hasnan NSN et al (2020) Recent developments in methane decomposition over heterogeneous catalysts: an overview. Mater Renew Sustain Energy 9:8. https://doi.org/10.1007/s40243-020-00167-5
Hosseini SE, Wahid MA (2016) Hydrogen production from renewable and sustainable energy resources: promising green energy carrier for clean development. Renew Sustain Energy Rev 57:850–866. https://doi.org/10.1016/j.rser.2015.12.112
Ighalo JO, Amama PB (2024) Recent advances in the catalysis of steam reforming of methane (SRM). Int J Hydrog Energy 51:688–700. https://doi.org/10.1016/j.ijhydene.2023.10.177
IRENA (2019) Hydrogen: a renewable energy perspective. IRENA, Tokyo
Karaismailoglu M et al (2019) Hydrogen production by catalytic methane decomposition over yttria doped nickel based catalysts. Int J Hydrog Energy 44:9922–9929. https://doi.org/10.1016/j.ijhydene.2018.12.214
Karaismailoglu M et al (2020) Methane decomposition over Fe-based catalysts. Int J Hydrog Energy 45:34773–34782. https://doi.org/10.1016/j.ijhydene.2020.07.219
Keipi T et al (2018) Economic analysis of hydrogen production by methane thermal decomposition: comparison to competing technologies. Energy Convers Manage 159:264–273. https://doi.org/10.1016/j.enconman.2017.12.063
Khojasteh Salkuyeh Y et al (2017) Techno-economic analysis and life cycle assessment of hydrogen production from natural gas using current and emerging technologies. Int J Hydrog Energy 42:18894–18909. https://doi.org/10.1016/j.ijhydene.2017.05.219
Kreutz T et al (2005) Co-production of hydrogen, electricity and CO_2 from coal with commercially ready technology. Part B: economic analysis. Int J Hydrog Energy 30:769–784. https://doi.org/10.1016/j.ijhydene.2004.08.001
Kumar S et al (2009) Hydrogen production by partial oxidation of methane: modeling and simulation. Int J Hydrog Energy 34:6655–6668. https://doi.org/10.1016/j.ijhydene.2009.06.043
Lamacz A (2019) CNT and H_2 production during CH_4 decomposition over Ni/$CeZrO_2$. I. A mechanistic study. ChemEngineering 3:26
Lane J, Spath P (2018) Technoeconomic analysis of the thermocatalytic decomposition of natural gas. National Renewable Energy Laboratory, Golden
Lepage T et al (2021) Biomass-to-hydrogen: a review of main routes production, processes evaluation and techno-economical assessment. Biomass Bioenergy 144:105920. https://doi.org/10.1016/j.biombioe.2020.105920
Levene JBK, Sverdrup G (2006) Wind energy and production of hydrogen and electricty—opportunities for renewable hydrogen. National Renewable Energy Laboratory (NREL), Golden
Li Y et al (2011) Methane decomposition to COx-free hydrogen and nano-carbon material on group 8–10 base metal catalysts: a review. Catal Today 162:1–48. https://doi.org/10.1016/j.cattod.2010.12.042
Li J et al (2016) Methane decomposition over high-loaded Ni–Cu–SiO_2 catalysts. Fusion Eng Des 113:279–287. https://doi.org/10.1016/j.fusengdes.2016.06.046
Li J et al (2017) Evolution of the Ni–Cu–SiO_2 catalyst for methane decomposition to prepare hydrogen. Fusion Eng Des 125:593–602. https://doi.org/10.1016/j.fusengdes.2017.05.040
Li G et al (2020) Life cycle energy consumption and GHG emissions of biomass-to-hydrogen process in comparison with coal-to-hydrogen process. Energy 191:116588. https://doi.org/10.1016/j.energy.2019.116588
Liang W et al (2020) Revealing the effect of nickel particle size on carbon formation type in the methane decomposition reaction. Catalysts 10:890. https://doi.org/10.3390/catal10080890
Lim J et al (2023) Novel carbon-neutral hydrogen production process of steam methane reforming integrated with desalination wastewater-based CO_2 utilization. Desalination 548:116284. https://doi.org/10.1016/j.desal.2022.116284
Liu F et al (2018) Chemical looping hydrogen production using activated carbon and carbon black as multi-function carriers. Int J Hydrog Energy 43:5501–5511. https://doi.org/10.1016/j.ijhydene.2018.01.098
Mason JE (2007) World energy analysis: H_2 now or later? Energy Policy 35:1315–1329. https://doi.org/10.1016/j.enpol.2006.03.024
McHugh K et al (2005) Hydrogen production methods. MPR Associates Inc., Alexandria, p 41
Mitoura dos Santos Junior J et al (2022) An analysis of the methane cracking process for CO_2-free hydrogen production using thermodynamic methodologies. Methane 1:243–261. https://doi.org/10.3390/methane1040020
Molburg JC, Doctor RD (2003) Hydrogen from steam methane reforming with CO_2 capture. In: 20th Annual international Pittsburgh coal conference
Moliner R et al (2005) Thermocatalytic decomposition of methane over activated carbons: influence of textural properties and surface chemistry. Int J Hydrog Energy 30:293–300. https://doi.org/10.1016/j.ijhydene.2004.03.035
Mondal KC, Ramesh Chandran S (2014) Evaluation of the economic impact of hydrogen production by methane decomposition with steam reforming of methane process. Int J Hydrog Energy 39:9670–9674. https://doi.org/10.1016/j.ijhydene.2014.04.087
Mueller-Langer F et al (2007) Techno-economic assessment of hydrogen production processes for the hydrogen economy for the short and medium term. Int J Hydrog Energy 32:3797–3810. https://doi.org/10.1016/j.ijhydene.2007.05.027
Muradov N (2000) Thermocatalytic CO-free production of hydrogen from hydrocarbon fuels. In: Proceedings of the 2000 hydrogen program review. NREL/CP-570–28890
Muradov N (2001) Catalysis of methane decomposition over elemental carbon. Catal Commun 2:89–94. https://doi.org/10.1016/S1566-7367(01)00013-9
Muradov N et al (2005) Catalytic activity of carbons for methane decomposition reaction. Catal Today 102–103:225–233. https://doi.org/10.1016/j.cattod.2005.02.018
Németh M et al (2019) Hindered methane decomposition on a coke-resistant Ni-In/SiO_2 dry reforming catalyst. Catal Commun 118:56–59. https://doi.org/10.1016/j.catcom.2018.10.003
Nikolaidis P, Poullikkas A (2017) A comparative overview of hydrogen production processes. Renew Sustain Energy Rev 67:597–611. https://doi.org/10.1016/j.rser.2016.09.044
Osman AI et al (2022) Hydrogen production, storage, utilisation and environmental impacts: a review. Environ Chem Lett 20:153–188. https://doi.org/10.1007/s10311-021-01322-8
Osman AI et al (2023a) Materials, fuels, upgrading, economy, and life cycle assessment of the pyrolysis of algal and lignocellulosic biomass: a review. Environ Chem Lett 21:1419–1476. https://doi.org/10.1007/s10311-023-01573-7
Osman AI et al (2023b) Cost, environmental impact, and resilience of renewable energy under a changing climate: a review. Environ Chem Lett 21:741–764. https://doi.org/10.1007/s10311-022-01532-8
Osman AI et al (2023c) Biofuel production, hydrogen production and water remediation by photocatalysis, biocatalysis and

electrocatalysis. Environ Chem Lett 21:1315–1379. https://doi.org/10.1007/s10311-023-01581-7
Parkinson B et al (2017) Techno-economic analysis of methane pyrolysis in molten metals: decarbonizing natural gas. Chem Eng Technol 40:1022–1030. https://doi.org/10.1002/ceat.201600414
Parkinson B et al (2018) Hydrogen production using methane: techno-economics of decarbonizing fuels and chemicals. Int J Hydrog Energy 43:2540–2555. https://doi.org/10.1016/j.ijhydene.2017.12.081
Parkinson B et al (2019) Levelized cost of CO_2 mitigation from hydrogen production routes. Energy Environ Sci 12:19–40. https://doi.org/10.1039/C8EE02079E
Patel S et al (2020) Production of hydrogen by catalytic methane decomposition using biochar and activated char produced from biosolids pyrolysis. Int J Hydrog Energy 45:29978–29992. https://doi.org/10.1016/j.ijhydene.2020.08.036
Pham Minh D et al (2021) Review on the catalytic tri-reforming of methane—Part I: impact of operating conditions, catalyst deactivation and regeneration. Appl Catal A Gen 621:118202. https://doi.org/10.1016/j.apcata.2021.118202
Ping D et al (2016) Co-production of hydrogen and carbon nanotubes on nickel foam via methane catalytic decomposition. Appl Surf Sci 369:299–307. https://doi.org/10.1016/j.apsusc.2016.02.074
Pinilla JL et al (2007) Hydrogen production by thermo-catalytic decomposition of methane: regeneration of active carbons using CO_2. J Power Sources 169:103–109. https://doi.org/10.1016/j.jpowsour.2007.01.045
Pudukudy M et al (2015) Direct decomposition of methane over Pd promoted Ni/SBA-15 catalysts. Appl Surf Sci 353:127–136. https://doi.org/10.1016/j.apsusc.2015.06.073
Pudukudy M et al (2016) Non-oxidative thermocatalytic decomposition of methane into COx free hydrogen and nanocarbon over unsupported porous NiO and Fe_2O_3 catalysts. Int J Hydrog Energy 41:18509–18521. https://doi.org/10.1016/j.ijhydene.2016.08.160
Pudukudy M et al (2017) One-pot sol-gel synthesis of MgO nanoparticles supported nickel and iron catalysts for undiluted methane decomposition into COx free hydrogen and nanocarbon. Appl Catal B Environ 218:298–316. https://doi.org/10.1016/j.apcatb.2017.04.070
Pudukudy M et al (2018) Catalytic decomposition of undiluted methane into hydrogen and carbon nanotubes over Pt promoted Ni/CeO_2 catalysts. New J Chem 42:14843–14856. https://doi.org/10.1039/C8NJ02842G
Pudukudy M et al (2019) Catalytic decomposition of methane over rare earth metal (Ce and La) oxides supported iron catalysts. Appl Surf Sci 467–468:236–248. https://doi.org/10.1016/j.apsusc.2018.10.122
Qian JX et al (2019) Optimization of a fluidized bed reactor for methane decomposition over Fe/Al_2O_3 catalysts: activity and regeneration studies. Int J Hydrog Energy 44:31700–31711. https://doi.org/10.1016/j.ijhydene.2019.10.058
Qian JX et al (2020) Methane decomposition to pure hydrogen and carbon nano materials: state-of-the-art and future perspectives. Int J Hydrog Energy 45:15721–15743. https://doi.org/10.1016/j.ijhydene.2020.04.100
Rahman MS et al (2006) Catalytic decomposition of methane for hydrogen production. Top Catal 37:137–145. https://doi.org/10.1007/s11244-006-0015-8
Ramasubramanian V et al (2020) Hydrogen production by catalytic decomposition of methane over Fe based bi-metallic catalysts supported on CeO_2–ZrO_2. Int J Hydrog Energy 45:12026–12036. https://doi.org/10.1016/j.ijhydene.2020.02.170
Ramsden T, Ruth M, Diakov V, Laffen M, Timbario TA (2013) Hydrogen pathways updated cost, well-to-wheels energy use, and emissions for the current technology status of ten hydrogen production, delivery, and distribution scenarios. National Renewable Energy Laboratory (NREL), Golden
Rastegarpanah A et al (2017a) Thermocatalytic decomposition of methane over mesoporous nanocrystalline promoted Ni/MgO·Al_2O_3 catalysts. Int J Hydrog Energy 42:16476–16488. https://doi.org/10.1016/j.ijhydene.2017.05.044
Rastegarpanah A et al (2017b) COx-free hydrogen and carbon nanofibers production by thermocatalytic decomposition of methane over mesoporous MgO·Al_2O_3 nanopowder-supported nickel catalysts. Fuel Process Technol 167:250–262. https://doi.org/10.1016/j.fuproc.2017.07.010
Rategarpanah A et al (2018) Thermocatalytic conversion of methane to highly pure hydrogen over Ni–Cu/MgO·Al_2O_3 catalysts: influence of noble metals (Pt and Pd) on the catalytic activity and stability. Energy Convers Manag 166:268–280. https://doi.org/10.1016/j.enconman.2018.04.033
Saha JK, Dutta A (2022) A review of graphene: material synthesis from biomass sources. Waste Biomass Valoriz 13:1385–1429. https://doi.org/10.1007/s12649-021-01577-w
Salam MA, Abdullah B (2017) Catalysis mechanism of Pd-promoted ?-alumina in the thermal decomposition of methane to hydrogen: a density functional theory study. Mater Chem Phys 188:18–23. https://doi.org/10.1016/j.matchemphys.2016.12.022
Sánchez-Bastardo N et al (2021) Methane pyrolysis for zero-emission hydrogen production: a potential bridge technology from fossil fuels to a renewable and sustainable hydrogen economy. Ind Eng Chem Res 60:11855–11881. https://doi.org/10.1021/acs.iecr.1c01679
Saraswat SK, Pant KK (2011) Ni–Cu–Zn/MCM-22 catalysts for simultaneous production of hydrogen and multiwall carbon nanotubes via thermo-catalytic decomposition of methane. Int J Hydrog Energy 36:13352–13360. https://doi.org/10.1016/j.ijhydene.2011.07.102
Saraswat SK, Pant KK (2013a) Synthesis of carbon nanotubes by thermo catalytic decomposition of methane over Cu and Zn promoted Ni/MCM-22 catalyst. J Environ Chem Eng 1:746–754. https://doi.org/10.1016/j.jece.2013.07.009
Saraswat SK, Pant KK (2013b) Synthesis of hydrogen and carbon nanotubes over copper promoted Ni/SiO_2 catalyst by thermocatalytic decomposition of methane. J Nat Gas Sci Eng 13:52–59. https://doi.org/10.1016/j.jngse.2013.04.001
Sgouridis S et al (2019) Comparative net energy analysis of renewable electricity and carbon capture and storage. Nat Energy. https://doi.org/10.1038/s41560-019-0365-7
Shen Y, Lua AC (2015) Sol–gel synthesis of titanium oxide supported nickel catalysts for hydrogen and carbon production by methane decomposition. J Power Sources 280:467–475. https://doi.org/10.1016/j.jpowsour.2015.01.057
Shilapuram V et al (2014) Hydrogen production from catalytic decomposition of methane over ordered mesoporous carbons (CMK-3) and carbide-derived carbon (DUT-19). Carbon 67:377–389. https://doi.org/10.1016/j.carbon.2013.10.008
Silva RRCM et al (2016) Effect of support on methane decomposition for hydrogen production over cobalt catalysts. Int J Hydrog Energy 41:6763–6772. https://doi.org/10.1016/j.ijhydene.2016.02.101
Simbeck DEC (2002) Hydrogen supply: cost estimate for hydrogen pathways—scoping anlysis. National Renewable Energy Laboratory (NREL). https://www.nrel.gov/docs/fy03osti/32525.pdf
Sisáková K et al (2019) Methane decomposition over modified carbon fibers as effective catalysts for hydrogen production. Catal Lett 150:781–793. https://doi.org/10.1007/s10562-019-02962-w
Srilatha K et al (2016) Hydrogen production using thermocatalytic decomposition of methane on Ni_{30}/activated carbon and Ni_{30}/carbon black. Environ Sci Pollut Res Int 23:9303–9311. https://doi.org/10.1007/s11356-015-5112-4

Srilatha K et al (2018) Comparison study between Ni/TiO_2 and Ni/flame synthesized TiO_2 catalysts for hydrogen production using thermocatalytic decomposition of methane. S Afr J Chem Eng 25:91–97. https://doi.org/10.1016/j.sajce.2018.02.003

Suelves I et al (2007) Hydrogen production by methane decarbonization: carbonaceous catalysts. Int J Hydrog Energy 32:3320–3326. https://doi.org/10.1016/j.ijhydene.2007.05.028

Takenaka S et al (2001) Decomposition of methane over supported-Ni catalysts: effects of the supports on the catalytic lifetime. Appl Catal A Gen 217:101–110. https://doi.org/10.1016/S0926-860X(01)00593-2

Tezel E et al (2019) Hydrogen production by methane decomposition using bimetallic Ni–Fe catalysts. Int J Hydrog Energy 44:9930–9940. https://doi.org/10.1016/j.ijhydene.2018.12.151

Torres D et al (2012) Hydrogen production by catalytic decomposition of methane using a Fe-based catalyst in a fluidized bed reactor. J Nat Gas Chem 21:367–373. https://doi.org/10.1016/S1003-9953(11)60378-2

Torres D et al (2014) Hydrogen and multiwall carbon nanotubes production by catalytic decomposition of methane: thermogravimetric analysis and scaling-up of Fe–Mo catalysts. Int J Hydrog Energy 39:3698–3709. https://doi.org/10.1016/j.ijhydene.2013.12.127

Torres D et al (2018a) Screening of Ni-Cu bimetallic catalysts for hydrogen and carbon nanofilaments production via catalytic decomposition of methane. Appl Catal A Gen 559:10–19. https://doi.org/10.1016/j.apcata.2018.04.011

Torres D et al (2018b) Co-, Cu- and Fe-doped Ni/Al_2O_3 catalysts for the catalytic decomposition of methane into hydrogen and carbon nanofibers. Catalysts 8:300. https://doi.org/10.3390/catal8080300

Torres D et al (2020) Cobalt doping of a-Fe/Al_2O_3 catalysts for the production of hydrogen and high-quality carbon nanotubes by thermal decomposition of methane. Int J Hydrog Energy 45:19313–19323. https://doi.org/10.1016/j.ijhydene.2020.05.104

Villacampa JI et al (2003) Catalytic decomposition of methane over Ni–Al_2O_3 coprecipitated catalysts: reaction and regeneration studies. Appl Catal A Gen 252:363–383. https://doi.org/10.1016/S0926-860X(03)00492-7

Voitic G, Hacker V (2016) Recent advancements in chemical looping water splitting for the production of hydrogen. RSC Adv 6:98267–98296. https://doi.org/10.1039/C6RA21180A

Wang J et al (2017) Preparation of Fe-doped carbon catalyst for methane decomposition to hydrogen. Ind Eng Chem Res 56:11021–11027. https://doi.org/10.1021/acs.iecr.7b02394

Wang D et al (2020) Methane thermocatalytic decomposition to COx-free hydrogen and carbon nanomaterials over Ni–Mn–Ru/Al_2O_3 catalysts. Int J Hydrog Energy 45:30431–30442. https://doi.org/10.1016/j.ijhydene.2020.08.039

Wibowo H et al (2021) Recent developments of deep eutectic solvent as absorbent for CO_2 removal from syngas produced from gasification: current status, challenges, and further research. J Environ Chem Eng 9:105439. https://doi.org/10.1016/j.jece.2021.105439

Yang C, Ogden J (2007) Determining the lowest-cost hydrogen delivery mode. Int J Hydrog Energy 32:268–286. https://doi.org/10.1016/j.ijhydene.2006.05.009

Yang L et al (2020) Joint-use of activated carbon and carbon black to enhance catalytic stability during chemical looping methane decomposition process. Int J Hydrog Energy 45:13245–13255. https://doi.org/10.1016/j.ijhydene.2020.03.055

Yao J et al (2017) Techno-economic assessment of hydrogen production based on dual fluidized bed biomass steam gasification, biogas steam reforming, and alkaline water electrolysis processes. Energy Convers Manag 145:278–292. https://doi.org/10.1016/j.enconman.2017.04.084

Yousefi Rizi HA, Shin D (2022) Green hydrogen production technologies from ammonia cracking. Energies 15:8246

Yuan W et al (2008) Economic analysis and process integration of hydrogen production strategies. In: Braunschweig B, Joulia X (eds) Computer aided chemical engineering. Elsevier, Amsterdam, pp 1083–1088. https://doi.org/10.1016/S1570-7946(08)80187-3

Zhang T, Amiridis MD (1998) Hydrogen production via the direct cracking of methane over silica-supported nickel catalysts. Appl Catal A Gen 167:161–172. https://doi.org/10.1016/S0926-860X(97)00143-9

Zhang Y, Smith KJ (2004) carbon formation thresholds and catalyst deactivation during CH_4 decomposition on supported Co and Ni catalysts. Catal Let 95:7–12. https://doi.org/10.1023/B:CATL.0000023714.69741.1d

Zhang W et al (2011) Influences of reaction conditions on methane decomposition over non-supported Ni catalyst. J Nat Gas Chem 20:339–344. https://doi.org/10.1016/S1003-9953(10)60205-8

Zhang J et al (2017) Hydrogen production by catalytic methane decomposition: carbon materials as catalysts or catalyst supports. Int J Hydrog Energy 42:19755–19775. https://doi.org/10.1016/j.ijhydene.2017.06.197

Zhang J et al (2018) Handy synthesis of robust Ni/carbon catalysts for methane decomposition by selective gasification of pine sawdust. Int J Hydrog Energy 43:19414–19419. https://doi.org/10.1016/j.ijhydene.2018.08.207

Zhang C et al (2022) Economic competitiveness of compact steam methane reforming technology for on-site hydrogen supply: a Foshan case study. Int J Hydrog Energy 47:32359–32371. https://doi.org/10.1016/j.ijhydene.2022.07.149

Zhou L et al (2017) Fe catalysts for methane decomposition to produce hydrogen and carbon nano materials. Appl Catal B Environ 208:44–59. https://doi.org/10.1016/j.apcatb.2017.02.052